Robotica (2016) volume 34, pp. 2689–2728. © Cambridge University Press 2015
doi:10.1017/S0263574715000302

Design, testing and evaluation of an end-effector for self-relocation

Feng Han*, Kui Sun, Yu Liu and Hong Liu

State Key Laboratory of Robotics and System, Harbin Institute of Technology, Harbin 150080, P. R. China

(Accepted April 16, 2015. First published online: July 3, 2015)

SUMMARY

Two identical end-effectors are indispensable for self-relocation of a space manipulator, which is an effective way of extending its servicing capability. The prototype design is intimately linked to the requirements. The significant features and functionality of the end-effector and its grapple fixture are described, including the key analysis efforts. The characteristics of the end-effector and their suitability for self-relocation and payload handling were confirmed by testing, which used two prototype end-effectors, a semi-physical simulation testbed system with two, six degrees of freedom (DOF) industrial robot arms, and an air-bearing testbed system with a seven DOF manipulator. The results demonstrate that the end-effector satisfies the requirements and it can work well in a simulated space environment. With the compliance motion of the manipulator, the end-effector can perform soft capture and the manipulator can securely self-relocate and handle the payload.

KEYWORDS: End-effector; Self-relocation; Servicing capability; Space manipulator; Capture misalignment envelope.

1. Introduction

The space manipulator is a very important tool for On-Orbit Servicing (OOS),[1–4] and its servicing capability has been demonstrated.[5–8] To complement the length limitation and extend its utility, one of the solutions is to give the space manipulator self-relocation capabilities.[9] The self-relocating manipulator is symmetric about its elbow with two identical three DOF shoulder and wrist clusters, including two identical end-effectors. Each cluster has three mechanical joints with perpendicular rotation axes. The end-effector is attached to the end of each cluster. The grapple fixtures spread throughout the space station exterior and act as basepoints. Being attached to the grapple fixture, the manipulator can step over from one basepoint to another or "walking", also called perform inchworm-like movement.[10,11] The end-effector at the tip of the manipulator acts as a hand for capture. The one at the base provides mechanical and electrical connections to the space station for manipulator support and operation. Therefore, the end-effector forms a key part of the self-relocating manipulator.

Among those end-effectors applied to space servicing, there are three for self-relocation, the Latching End-effector (LEE),[12,13] the Basic End-effector (BEE)[14] and the reflector assembly end-effector.[15]

The LEE is attached to the two ends of the Space Station Remote Manipulator System (SSRMS) which is mainly used for the International Space Station (ISS) assembly.[16–18] The LEE can perform soft capture and hard docking. Its capture misalignment envelope is large(dx/±100 mm; dy/±100 mm; dz/0∼100 mm; Yaw($d\psi$)/±15°; Pitch($d\theta$)/±15°; Roll($d\varphi$)/±10°). The LEE has a three-cable snare mechanism, a rigidizing mechanism, four latching and umbilical mechanisms, an EVA (Extra Vehicular Activity) drive, and a force moment sensor. In the rigidizing mechanism and the latching mechanism, the spring systems are used to achieve constant preload. The mechanical power provision and dexterous task performance are realized by the Special Purpose Dexterous Manipulator (SPDM)

* Corresponding author. E-mail: hf09122@yahoo.com

and its ORU (Orbital Replaceable Unit) Tool Change-out Mechanism (OTCM), together with its tools.[19,20]

The BEE is attached to the two ends of the European Robotic Arm (ERA) which is used on the Russian segment of the ISS.[21] With the force moment sensor steering and the leading edge being carefully designed, the BEE can perform soft capture by managing the capture force and moment within 20 N and 20 N•m, respectively. Its capture misalignment envelope is small(dx/±25 mm; dy/±25 mm; dz/±25 mm; Yaw($d\psi$)/±3°; Pitch($d\theta$)/±3°; Roll($d\varphi$)/±3°). The BEE has a three-hook/lever-system grapple mechanism, a connector unit, an EVA drive, a force moment sensor, and a mechanical power output chain. The hook is preloaded by coil springs with 30 N. The rigidization is implemented by over-centering. Because the hooks are internal jaws, the capture misalignment envelope is limited by both the outside diameter of the grapple fixture and the integration of the grapple and rigidizing mechanisms. Besides, without any flexible elements, the preload in the grapple hook is sensitive to small variation in dimensions and thermal distortion. These disadvantages are solved by the upgraded Capture Tool.[22] The dexterous tasks performance is realized by EUROBOT and its end-effectors and tools.[23,24]

The reflector assembly end-effector is attached to the two ends of a small space self-relocating manipulator, which is used for on-orbit assembly of a large telescope reflector. The end-effector comprises a mechanical power output chain and a clip type grasping mechanism integrated with an electrical connection mechanism. For both grapple fixtures, the positional misalignment envelope is 10 mm or more in the X and Y directions.

Besides the aforementioned, end-effectors of the fixed space manipulators are worthwhile,[25–44] together with the docking system of the Orbital Express (OE),[45–49] and the Exposed Facility Berthing Mechanism (EFBM) and the Equipment Exchange Unit (EEU) of the Exposed Facility (EF).[50] The docking system is used for satellite docking. It has three grappling fingers for capture and three dampers for soft docking. The rigidizaiton is realized by the grappling fingers preloaded by the motor. By the EFBM, the EF is attached to the Pressurized Module. The EFBM comprises four grappling fingers for large load capture, latching and release. Via the EEU, the EF payloads are attached to the EF. The EEU consists of three grappling fingers for capture, rigidization and release.

To extend the space servicing capability, a self-relocating manipulator was developed, which needs two identical end-effectors for self-relocation and payload handling. In this research, the end-effector was developed. In Section 2, the prototype design of end-effector and its grapple fixture is presented. In Section 3, the main analytic efforts of the characteristics are presented. In Section 4, the capture misalignment envelope is achieved by analysis and simulation. The experiments are presented in Section 5, followed by the conclusions.

2. Requirement, Function Analysis and Structure Design of End-effector and Grapple Fixture

As shown in Fig. 1, the space manipulator is symmetric about its elbow and has two identical end-effectors. The end-effector is used to support the self-relocation and payload handling of the manipulator. Its design is dominated by the requirements arising from the manipulator, task, worksite and environment. The prototype design involves requirement, function analysis, structure design of the end-effector and its grapple fixture, and the capture process.

2.1. Requirements

The performance index of the end-effector are shown in Table I. The principal function requirements are listed below:

(1) To support the self-relocating capability of the manipulator;
(2) To perform soft docking and soft capture under the compliance control of the manipulator;
(3) To act equally as a wrist and shoulder unit;
(4) Provision of power, data, signal and video transmission across the mating surface;
(5) Provision of mechanical power with a standard interface such as M10 hexagonal bolt head and socket, the drive shaft locates at the center of the end-effector;
(6) High strength, stiffness, reliability and long life, whether it acts as a shoulder base or wrist hand;
(7) Provision of manual release and EVA drive;

https://doi.org/10.1017/S0263574715000302 Published online by Cambridge University Press

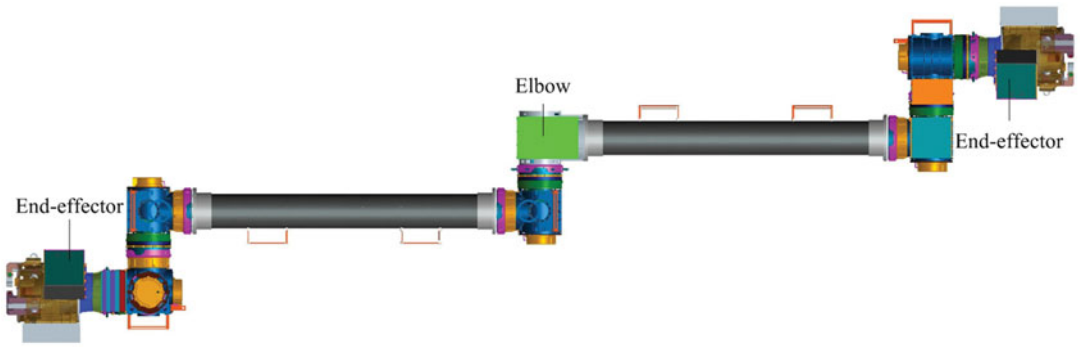

Fig. 1. Space manipulator.

Table I. Performance index of the end-effector.

Number	Item		Value
1	Size/mm		<Φ330*400
2	Grapple fixtures/kg		<8
3	Mass/kg		<35
4	Output torque/(N•m)		>40
5	Preload/N		≥12,000
6	Capture and latching time/s		<240
7	Operation times		>1000
8	Positional misalignment/mm	*dx*	≥40
		dy	
		dz	
	Angular misalignment/(°)	*Yaw*/$d\psi$	≥4
		Pitch/$d\theta$	
		Roll/$d\varphi$	

(8) Force moment sensor;
(9) The end-effector must be modular and designed as an ORU.

In addition, there are some specific safety requirements of the end-effector as below:

(1) The capture must be successful every time;
The end-effector must be able to grasp the grapple fixture even though a misalignment between the end-effector and the grapple fixture exists, and even before it is calibrated.

(2) The end-effector must have emergency release capability;
If a large external force would act on the capture fingers, they must be able to release the grapple fixture rapidly before the completion of the grappling operation. This would prevent the capture fingers from damage.

(3) For payload transfer, one end-effector attached to the grapple fixture acts as a shoulder base, and the other acts as a hand for payload holding. If there is a large external force would apply to the payload, the shoulder base end-effector must be able to stably grasp the grapple fixture mounted on the base, the wrist end-effector must be able to simultaneously hold the payload so that it cannot become debris in space.
(4) The end-effector and the grapple fixture with payload must be able to be released by the astronauts EVA if any inadvertence happens.

2.2. Function analysis

According to the requirements, the functions of the end-effector assembly are subdivided. The evaluations and trade-off studies of the main function schemes are as follows:

https://doi.org/10.1017/S0263574715000302 Published online by Cambridge University Press

(1) Capture
The capture capability of the end-effector is very important for OOS. There are many capture methods, among them five different schemes are evaluated:
(a) Cables-probe capture;
(b) Fingers-(flexible) probe-ball capture;
(c) Cone-probe capture;
(d) Fingers deployment capture;
(e) Fingers closure enveloping capture.
The methods (a), (b) and (c) can achieve a good capture capability, but they cannot realize the mechanical power output because of the probe. As for the method (d), the capture envelope is limited by the outside diameter of the grapple fixture. The deficiencies of the methods (a), (b), (c) and (d) can be complemented by the method (e). As a result, the capture is based on the enveloping capture with fingers. After further comparison and extensive evaluation, three capture fingers and a trefoil are selected as the capture strategy of the end-effector. The synchronization of the three capture fingers is achieved by their synchronous actuation. And it is established at assembly.

(2) Retraction
The reeling back and ball screw are usually used for retraction. The reeling back scheme will increase complications. Instead, with the successful application experience in space, the retraction is implemented by the ball screw and nut.

(3) Rigidization
The predecessors of the end-effector perform rigidization by either the latching mechanisms with an individual drive or the integrated grappling mechanism. The former adds mass and complications to the end-effector, while the latter sacrifices the capture capability envelope. Synthesizing the two methods, a mechanical linking scheme is proposed, which simplifies the mechanism and simultaneously makes the capture and latching functions separate.

(4) Interchangeable manipulator interface
The end-effector is an ORU and all the interchangeable interfaces of the manipulator are uniform and standard.

(5) Interface stiffness
To enhance the interface stiffness, the load paths are refined to pass only along the shell of end-effector. And the wide contact surface between the end-effector and the grapple fixture is employed to enhance the interface stiffness.
As a result, the end-effector and its grapple fixture are designed based on the corresponding function schemes, as shown in Fig. 2. The end-effector has three capture fingers and three sets of latching mechanisms. The grapple fixture is a trefoil structure.

2.3. Structure design of end-effector

As shown in Fig. 3, the end-effector consists of a cover plate subassembly, a canister subassembly, a force moment sensor and a manipulator interface. The cover plate subassembly is attached to the canister subassembly under which is a force moment sensor and a manipulator interface in turn. Within the canister subassembly is a capture drive chain, a mechanical power output chain, and an EVA drive mechanism. On the exterior surface of the canister subassembly is a hand-eye camera and an electrical control box (Fig. 2).

The cover plate subassembly is used for alignment and engagement between the end-effector and the grapple fixture. It has a cover plate on which are three electrical connectors, three curvic teeth, three break switches and three positioning struts. Each strut is integrated with a spring-damper system for soft docking.

The capture drive chain provides capture operation and drive. It contains a brushless DC motor, a gear cluster, a ball screw and nut, a force sensor, a linear position sensor, three capture fingers and three sets of latching mechanisms. The force sensor measures the applied force on the screw, while the linear position sensor measures the nut position. The three capture fingers are axisymmetrically attached to the nut and simultaneously restricted on the three guide pins via their sliding groove. The

https://doi.org/10.1017/S0263574715000302 Published online by Cambridge University Press

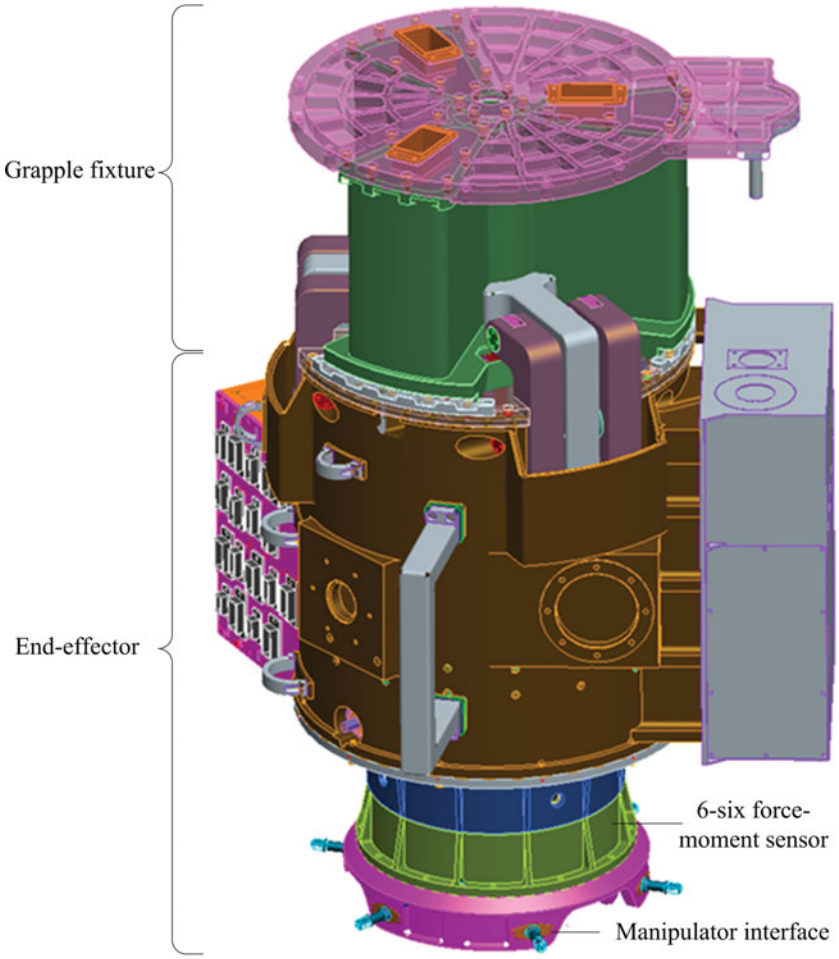

Fig. 2. End-effector and grapple fixture.

latching mechanism is also installed on the guiding pin and can rotate around it. It is symmetric about the capture finger.

As shown in Fig. 4, the capture finger and the latching mechanism constitute a linkage mechanism. The capture finger can only slide on the guide pin and drives the latching mechanism rotation via the engagement between the linking hook and the linking shaft. To engage successfully every time, the return springs are employed to make the linking shaft return back to its initial position where it is within the capture capability of the linking hook. The return springs are used to make the latching fingers return back to their initial position where they are in contact with the shell.

The mechanical power output chain is used to provide mechanical power to fasten/unfasten the payload. It contains a brushless DC motor, a gear cluster, a drive shaft with a M10 hexagonal bolt socket. The shaft is inside the hollow screw, and they are coaxial.

2.4. Structure design of grapple fixture

As shown in Fig. 5, the grapple fixtures are trefoil. The large grapple fixture contains a trefoil body, a vision target, six elastic elements and three curvic teeth. The trefoil body integrates a cylinder, an interface plate and three wedges. All the wedge surfaces intersect the cylindrical surface. The grapple fixture has three capture feature spaces corresponding to the capture finger tips. The elastic elements are used to produce the constant deformation preload for rigidization and simultaneously absorb the errors in assembly, structural and thermal distortions during the operation. The small grapple fixture has a trefoil body and a vision target. It is attached to small and light payloads, and its preload is performed by the capture fingers.

https://doi.org/10.1017/S0263574715000302 Published online by Cambridge University Press

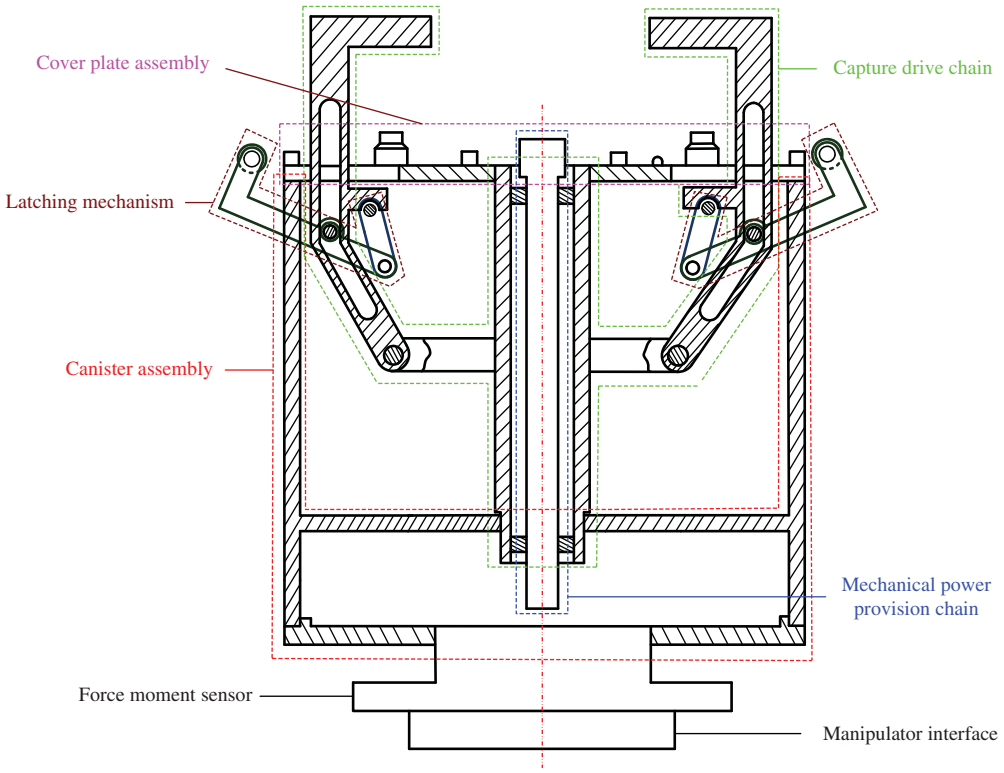

Fig. 3. End-effector cross-section.

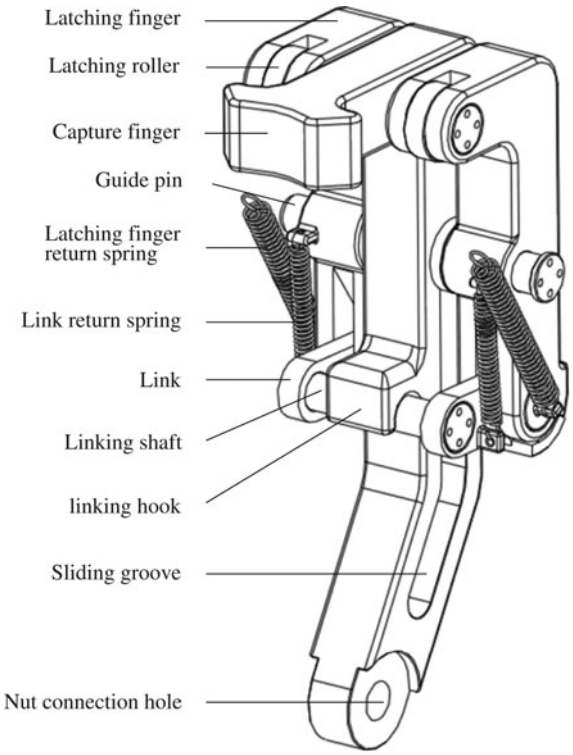

Fig. 4. Linkage mechanism.

https://doi.org/10.1017/S0263574715000302 Published online by Cambridge University Press

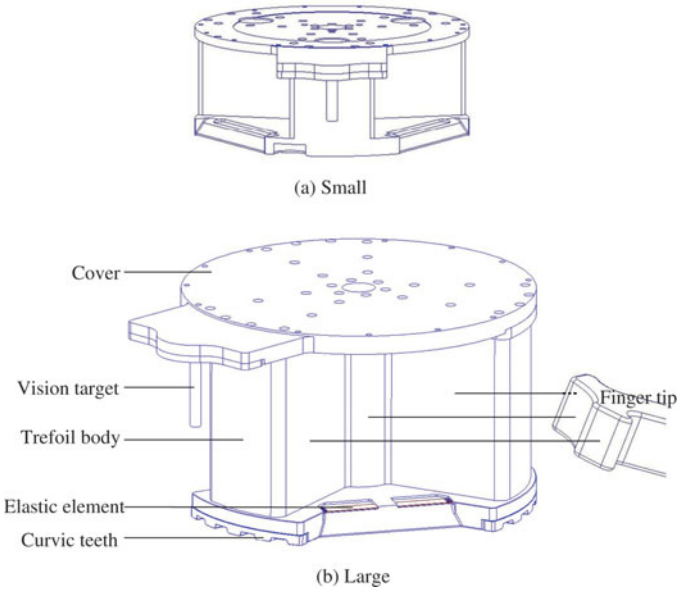

Fig. 5. Grapple fixture.

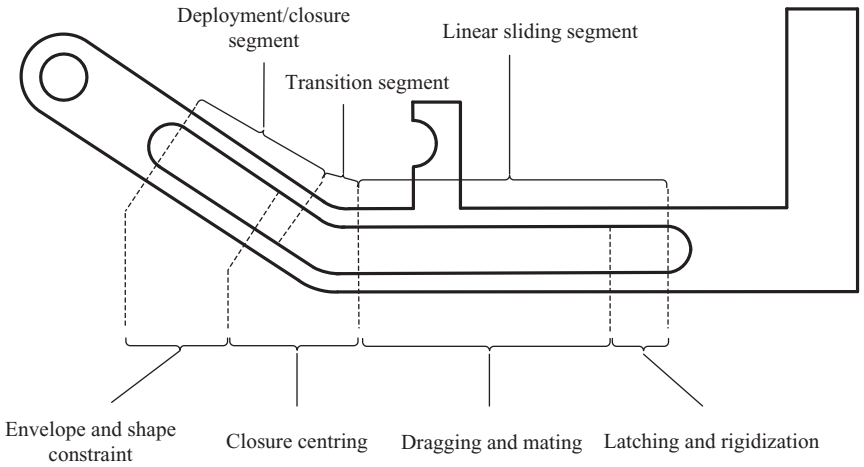

Fig. 6. Relationship between the capture process and sliding groove.

2.5. Capture process

The capture process corresponds to the sliding groove of the capture finger, as shown in Fig. 6. It contains capture positioning, envelope and shape constraint, closure centring, dragging and mating, latching and rigidization, as shown in Fig. 7.

(1) Capture positioning
The capture fingers of the end-effector begin in a maximal deployed state and the latching mechanisms begin in the initial position. The end-effector is positioned where the fixed grapple fixture is within its capture capability.

(2) Envelope and shape constraint
On receipt of command, the motor begins to actuate the ball screw which translates the nut along the length of the end-effector. The nut moves the three capture fingers. The capture fingers slide on the guide pins along the deployment/closure segment and close. The wedge shaped architecture of the grapple fixture guides the finger tips into the capture feature spaces. The capture is achieved as the grapple fixture is constrained within the boundary of the capture fingers.

https://doi.org/10.1017/S0263574715000302 Published online by Cambridge University Press

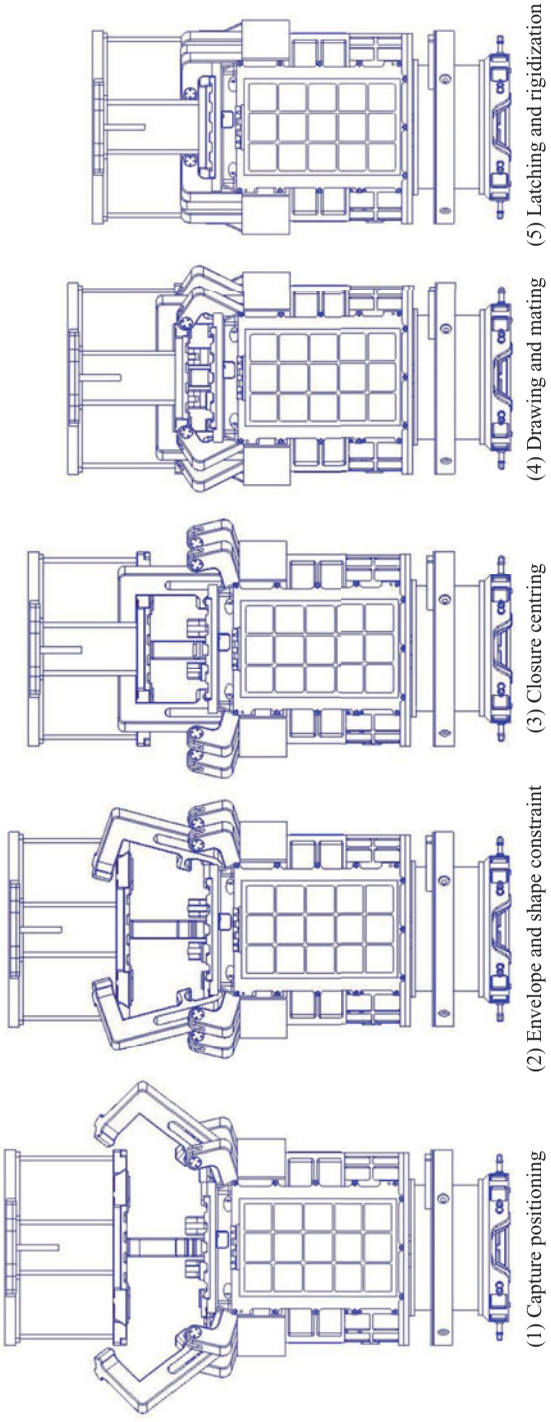

Fig. 7. Capture process.

https://doi.org/10.1017/S0263574715000302 Published online by Cambridge University Press

(3) Closure centring
The capture fingers continually slide throughout the transition segment. The capture finger tips engage with the capture feature spaces and center the grapple fixture. As a result, there only leaves an axial offset between the end-effector and grapple fixture.

(4) Dragging and mating
As the capture fingers slide along the linear sliding segment, their hooks engage with the interface plate and draw it down together. As retraction proceeds, the linking hooks begin to engage with the linking shafts, and then actuate the latching mechanisms rotation. Once the latching rollers contact with the interface plate, they actuate it to separate from the capture fingers and continually move down. When the three positioning struts enter the tapered pockets, a three-point alignment between the end-effector and the grapple fixture comes into being. With further retraction, the curvic teeth engage with each other for fine alignment. When the break switches send out indications, the engagement between the end-effector and the grapple fixture is complete. The grapple fixture is fully constrained.

(5) Latching and rigidization
The rigidization then occurs. The rotation of latching fingers causes the elastic elements to produce deformation. When all the latching fingers rotate to their final positions, the deformations are at their maximum value. The corresponding deformation load causes the end-effector and the grapple fixture to rigidize as a whole. At the same time, the capture fingers stop and the rigidization state is held.

At steps (2) and (3), the capture fingers independently capture the grapple fixture. At steps (4) and (5), the capture fingers actuate the latching mechanisms to rotate and latch the grapple fixture.

From the presentation above, it can conclude that the linkage mechanism is the key component of the end-effector and its motion corresponds to the capture process which will be reclassified and analyzed in the next section.

3. Linking Relationship during Capture, Dragging, Linkage, Latching and Release Phase

Section 2.5 shows that the capture process is a mechanical linking process relating to the grapple fixture, the capture finger and the latching mechanism. The linkage mechanism comes into being in the middle of the capture process, called middle process linking. According to the difference of the counterparts acting on the grapple fixture, the capture process is reclassified into a capture, dragging, linkage, latching and release phase. In each phase, their linking relationships are presented as follows.

3.1. Relationship during capture phase

The capture phase contains steps (2) and (3). During the phase, the capture fingers interact with the grapple fixture and the latching mechanisms are static. With simplification, the grapple fixture, the capture finger *ACFIGHN*, the link *MB*, and the latching finger *DEBJ* are shown in Fig. 8. The loop *GH* is the sliding groove and the included angle of its center lines *IQ* and *QN* is equal to 30°. The points *A*, *M*, and $J(m, -g)$ are the centers of the linking hook, linking shaft, and guide pin, respectively. The corresponding relations are listed as follows.

The dimensional relationships of the capture finger are

$$\begin{cases} d < a \\ e < b \end{cases}. \tag{1}$$

The dimensional relationships between the grapple fixture and the capture finger are

$$\begin{cases} d_1 < m < R_{\mathrm{E}} \\ m = a + R_1 \\ n < m \end{cases}. \tag{2}$$

When the centering exists, the line *GQ* is parallel to the *z*-axis and the linking hooks are over the cover plate. This condition is written as

$$\begin{cases} x_G = x_I = m \\ g < b - e \end{cases}. \tag{3}$$

https://doi.org/10.1017/S0263574715000302 Published online by Cambridge University Press

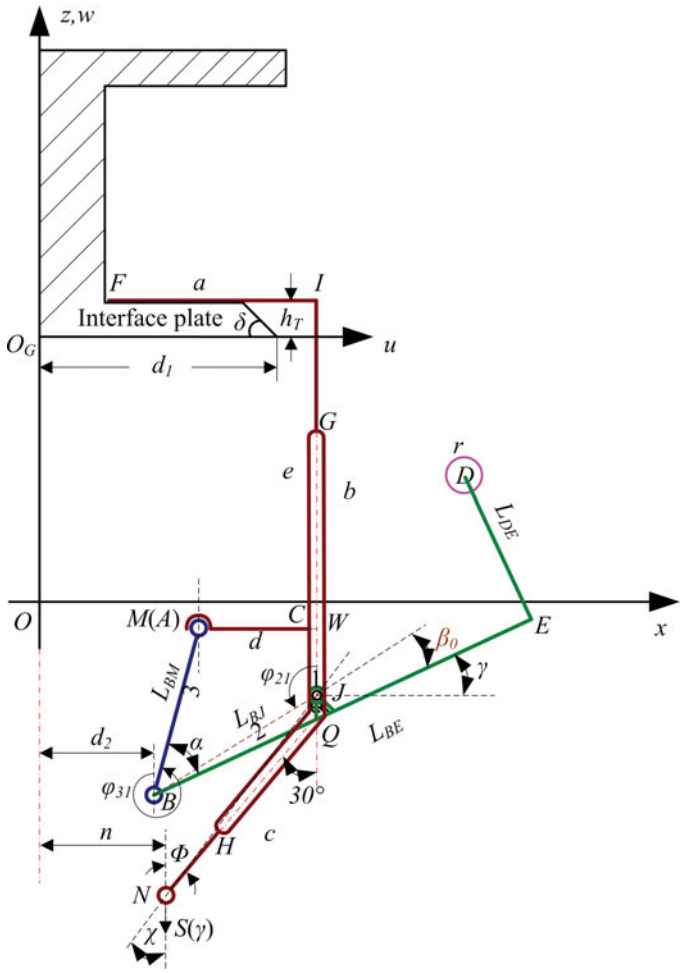

Fig. 8. Positional relationship among components.

The angles Φ and χ of the capture finger coincide, which is given by

$$\phi \equiv \chi . \tag{4}$$

The trajectory of the point N is parallel to the z-axis, which is given by

$$\begin{cases} x_N = n \\ z_N = -g - (m-n)\cot\chi \end{cases}. \tag{5}$$

The trajectory of the point F is obtained from the point N, which is given by

$$\begin{cases} x_F = n + c\sin\phi + b\sin(\phi - 30^\circ) - a\cos(\phi - 30^\circ) \\ z_F = -[g + (m-n)\cot\phi_0 + S_N] + c\cos\phi + b\cos(\phi - 30^\circ) + a\sin(\phi - 30^\circ) \end{cases}, \tag{6}$$

where $30^\circ \le \Phi \le \Phi_0 < 90^\circ$.

At any time, the displacement S_N of the point N can be measured by the linear position sensor, its velocity can be calculated by a data fusion algorithm. The displacement S_N can be used to solve the displacement of the capture finger which contains a sliding displacement S_{Fs} and an angular displacement Θ.

At any time, the displacement S_N is calculated as

$$S_N = (m-n)(\cot\chi - \cot\phi_0). \tag{7}$$

https://doi.org/10.1017/S0263574715000302 Published online by Cambridge University Press

Therefore, the sliding displacement S_{Fs} is

$$S_{Fs} = (m-n)\left(\frac{1}{\sin\chi} - \frac{1}{\sin\phi_0}\right). \tag{8}$$

And the angular displacement Θ is

$$\Theta = \phi_0 - \chi. \tag{9}$$

During the capture phase, the whole displacement S_{N1} of the point N is

$$S_{N1} = (m-n)\left(\sqrt{3} - \cot\phi_0\right). \tag{10}$$

The angular displacement $\Delta\gamma$ of the latching fingers is

$$\Delta\gamma \equiv 0. \tag{11}$$

The distance d_{GE1} between the grapple fixture and the end-effector is

$$d_{\mathrm{GE1}} = b - g - h_{\mathrm{T}}. \tag{12}$$

3.2. Relationship during dragging phase

The dragging phase is from the closure centring to the engagement of the linking hook with the linking shaft. It is the first segmentation of step (4). During this phase, the capture fingers retract and draw the grapple fixture down together while the latching mechanisms are still static.

Equation (3) shows that angle Φ is a constant and angle χ changes with the motion of the capture finger, which is given by

$$\begin{cases} \phi \equiv 30^\circ \\ \chi = \operatorname{arccot}\left(\frac{S_N}{m-n} + \cot\phi_0\right) \end{cases}. \tag{13}$$

During the dragging phase, the whole displacement S_{N2} is

$$S_{N2} = b - e + L_{BJ}\sin(\gamma_0+\beta_0) - \sqrt{L_{MB}^2 - (d - L_{BJ}\cos(\gamma_0+\beta_0))^2}. \tag{14}$$

The angular displacement $\Delta\gamma$ is

$$\Delta\gamma \equiv 0. \tag{15}$$

The distance d_{GE2} becomes

$$\begin{aligned} d_{\mathrm{GE2}} &= b - g - h_T - S_{N2} \\ &= e - g - h_T - \left(L_{BJ}\sin(\gamma_0+\beta_0) - \sqrt{L_{MB}^2 - (d - L_{BJ}\cos(\gamma_0+\beta_0))^2}\right). \end{aligned} \tag{16}$$

At the end of the dragging phase, the linking hook would engage with the linking shaft. The prerequisite of the engagement is that the linking shaft is always within capture capability of the linking hook, which is written as

$$\begin{cases} x_A \le x_M \le m \\ z_M \le z_A \end{cases}, \tag{17}$$

where $x_A = m - d$. With Eq. (3), the condition $z_M < z_A$ is always tenable and the prerequisite is reduced to

$$0 \le L_{JB}\cos(\beta_0+\gamma_0) - L_{MB}\cos(\alpha_0+\gamma_0) \le d. \tag{18}$$

https://doi.org/10.1017/S0263574715000302 Published online by Cambridge University Press

When at the moment of engagement, the point M and A coincide, which is described by

$$\begin{cases} x_M = x_A \\ z_M = z_A \end{cases} \Rightarrow \begin{cases} L_{BJ}\cos(\gamma+\beta_0) - L_{BM}\cos(\alpha+\gamma) = d \\ -L_{BJ}\sin(\gamma+\beta_0) + L_{BM}\sin(\alpha+\gamma) = -(m-n)\cot\chi + b + \frac{\sqrt{3}}{2}c - e \end{cases}. \tag{19}$$

And the capture finger and the latching mechanism constitute a linkage mechanism.

3.3. Relationship during linkage phase

The linkage phase is from the engagement to the beginning of the contact between the latching rollers and the grapple fixture. It is the second segmentation of step (4). During the phase, the capture fingers draw the grapple fixture and simultaneously drive the latching mechanisms rotation. With a simplification, the linkage mechanism *M(A)BJ* is similar to a rocker slider mechanism and has eccentricity d. The point A and the line segment BJ act as a slider and a rocker, respectively. Their corresponding relationships are presented as follows.

The line segment BJ is not a crank but a rocker, which is given by

$$L_{BJ} - L_{MB} < d. \tag{20}$$

The linkage mechanism can move, which is given by

$$d < L_{BJ} + L_{MB}. \tag{21}$$

The range of the link length L_{MB} can be calculated according to the initial position ($\alpha = \alpha_0$, $\gamma = \gamma_0$) and the latching position ($\alpha = \alpha_1 < 90^\circ$ and $\gamma = 90^\circ$) as

$$d + L_{BJ}\sin\beta_0 < L_{MB} < \frac{L_{BJ}\sin(\gamma_0+\beta_0) + g}{\sin(\gamma_0+\alpha_0)}. \tag{22}$$

The range of the rocker length L_{BJ} can be calculated according to the initial position ($\gamma = \gamma_0$) as

$$L_{BJ} < \frac{m - d_2}{\cos(\gamma_0+\beta_0)}. \tag{23}$$

To obtain the transfer function of the linkage mechanism, first presume that it is the rocker BJ that drives the slider (point A) and the corresponding transfer function $S(\gamma)$ is

$$S(\gamma) = L_{BJ}\sin(\gamma+\beta_0) \pm \sqrt{L_{MB}^2 - (d - L_{BJ}\cos(\gamma+\beta_0))^2}, \tag{24}$$

where the domain of the angle variable γ is the angular displacement of the latching fingers, $\gamma_0 \le \gamma \le 90^\circ$. Therefore, the transfer function $S(\gamma)$ is reduced to

$$S(\gamma) = L_{BJ}\sin(\gamma+\beta_0) - \sqrt{L_{MB}^2 - (d - L_{BJ}\cos(\gamma+\beta_0))^2}, \tag{25}$$

where $\gamma_0 \le \gamma \le 90^\circ$.

As shown in Fig. 9, the trajectory curve $S(\gamma)$ shows that it is a continuous, monotone function. Its inverse function $S^{-1}(s)$ is the transfer function of the linkage mechanism given as

$$S^{-1}(s) = \sec^{-1}\left(\frac{2L_{BJ}\left(d^2+s^2\right)}{d^3 + \sqrt{-s^2\left(d^2-(L_{BJ}-L_{BM})^2+s^2\right)\left(d^2-(L_{BJ}+L_{BM})^2+s^2\right)} + d\left(L_{BJ}^2 - L_{MB}^2 + s^2\right)}\right) - \beta_0 \tag{26}$$

https://doi.org/10.1017/S0263574715000302 Published online by Cambridge University Press

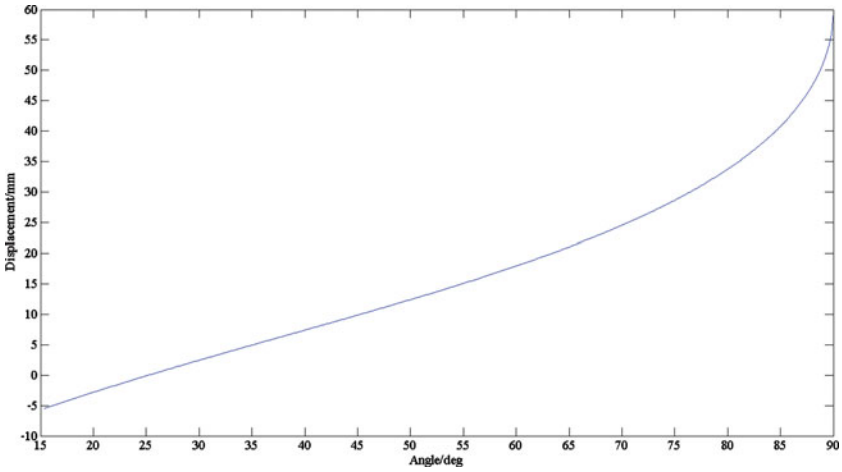

Fig. 9. Transfer function S(γ) curve.

where

$$L_{BJ}\sin(\gamma_0+\beta_0)-\sqrt{L_{MB}^2-(d-L_{BJ}\cos(\gamma_0+\beta_0))^2}$$
$$\le s \le L_{BJ}\cos\beta_0-\sqrt{L_{MB}^2-(d+L_{BJ}\sin\beta_0)^2}.$$

The displacement S_{N3} is

$$S_{N3}=\left(L_{BJ}\sin(\gamma_1+\beta_0)-\sqrt{L_{MB}^2-(d-L_{BJ}\cos(\gamma_1+\beta_0))^2}\right)$$
$$+\left(-L_{BJ}\sin(\gamma_0+\beta_0)+\sqrt{L_{MB}^2-(d-L_{BJ}\cos(\gamma_0+\beta_0))^2}\right). \quad (27)$$

The angular displacement $\Delta\gamma$ is

$$\Delta\gamma=\gamma_1-\gamma_0. \quad (28)$$

The distance d_{GE3} is

$$d_{\mathrm{GE3}}=b-g-h_T-S_{N2}-S_{N3}$$
$$=e-g-h_T-\left(L_{BJ}\sin(\gamma_1+\beta_0)-\sqrt{L_{MB}^2-(d-L_{BJ}\cos(\gamma_1+\beta_0))^2}\right). \quad (29)$$

The pressure angle α_{P} is

$$\alpha_{\mathrm{P}}=90^\circ-(\alpha-\beta_0). \quad (30)$$

The minimum driving angle $\gamma_{\min}$ is

$$\gamma_{\min}=\alpha_0-\beta_0. \quad (31)$$

The velocity and acceleration of the linkage mechanism can be calculated according to the closed vector polygon and its projection on the x-axis and the z-axis. The guide pin, rocker and link are numbered 1, 2 and 3, respectively (Fig. 8).

The vector equation of the closed polygon is

$$\vec{L}_{BJ}+\vec{L}_{BM}+\vec{d}+\vec{s}=0. \quad (32)$$

https://doi.org/10.1017/S0263574715000302 Published online by Cambridge University Press

And its projections on the x-axis and the z-axis are

$$\begin{cases} \sum X = 0 \Rightarrow L_{BJ} \sin \varphi_{21} + L_{BM} \sin \varphi_{31} + d = 0 \\ \sum Z = 0 \Rightarrow L_{BJ} \cos \varphi_{21} + L_{BM} \cos \varphi_{31} - s = 0 \end{cases} \tag{33}$$

where

$$\begin{aligned} \varphi_{21} &= 90^\circ + (\gamma + \beta_0) \\ \varphi_{31} &= 270^\circ + (\alpha + \gamma) \end{aligned}.$$

The time derivative of Eq. (33) is calculated to solve the angular velocity of members 2 and 3. The angular velocity of the rocker is

$$\dot{\varphi}_{21} = \dot{s} \frac{\cos \varphi_{31}}{L_{BJ} \sin (\varphi_{31} - \varphi_{21})}. \tag{34}$$

And the angular velocity of the link is

$$\dot{\varphi}_{31} = \dot{s} \frac{-\cos \varphi_{21}}{L_{BM} \sin (\varphi_{31} - \varphi_{21})}. \tag{35}$$

With Eqs. (34) and (35), the second derivative of Eq. (33) is calculated to solve the angular acceleration velocity of members 2 and 3. The angular acceleration of the rocker is

$$\ddot{\varphi}_{21} = \ddot{s} \frac{\cos \varphi_{31}}{L_{BJ} \sin (\varphi_{31} - \varphi_{21})} + \dot{s}^2 \left[\frac{\cos^2 \varphi_{21}}{L_{BJ} L_{BM}} + \frac{\cos^2 \varphi_{31}}{L_{BJ}^2} \cos (\varphi_{31} - \varphi_{21}) \right] \frac{1}{\sin^3 (\varphi_{31} - \varphi_{21})}. \tag{36}$$

And the angular acceleration of the link is

$$\ddot{\varphi}_{31} = -\ddot{s} \frac{\cos \varphi_{21}}{L_{BM} \sin (\varphi_{31} - \varphi_{21})} - \dot{s}^2 \left[\frac{\cos^2 \varphi_{31}}{L_{BM} L_{BJ}} + \frac{\cos^2 \varphi_{21}}{L_{BM}^2} \cos (\varphi_{31} - \varphi_{21}) \right] \frac{1}{\sin^3 (\varphi_{31} - \varphi_{21})}. \tag{37}$$

3.4. Relationship during latching phase

The latching phase is from the contact to the end of latching rigidization. It contains the final segmentation of step (4) and step (5). During the phase, the capture fingers separate from the grapple fixture and only drive the latching mechanisms, while the latch fingers interact with the grapple fixture. The latching phase consists of a latching capture, actuation apart and latching rigidization, as shown in Fig. 10. The corresponding relationships are presented as follows, including the latching dimensions, the capture force and latching force.

(1) Latching capture

The latching capture is where the latching fingers successfully capture the grapple fixture during rotation. It is the prerequisite of the latching. The critical condition of capture success is when the latching fingers rotate to the position where the latching rollers and the line $x = d_1$ are tangent at the point T, the mating surface of the interface plate is below, or at most horizontal to, the point T of tangency. This condition can be described by

$$\begin{cases} x_T = d_1 \\ z_T \geq d_{\mathrm{GE3}} \end{cases} \Rightarrow \begin{cases} \gamma_1 = 180^\circ - \theta_L - \arccos \left(\dfrac{m - r - d_1}{\sqrt{(L_{DE} - L_{BJ} \sin \beta_0)^2 + (L_{BE} - L_{BJ} \cos \beta_0)^2}} \right), \\ L_{BE} \sin \gamma_1 + L_{DE} \cos \gamma_1 \geq e - h_T + \sqrt{L_{MB}^2 - (d - L_{BJ} \cos (\gamma_1 + \beta_0))^2} \end{cases} \tag{38}$$

where $\theta_L = \arctan \left(\frac{L_{DE} - L_{BJ} \sin \beta_0}{L_{BE} - L_{BJ} \cos \beta_0} \right)$.

https://doi.org/10.1017/S0263574715000302 Published online by Cambridge University Press

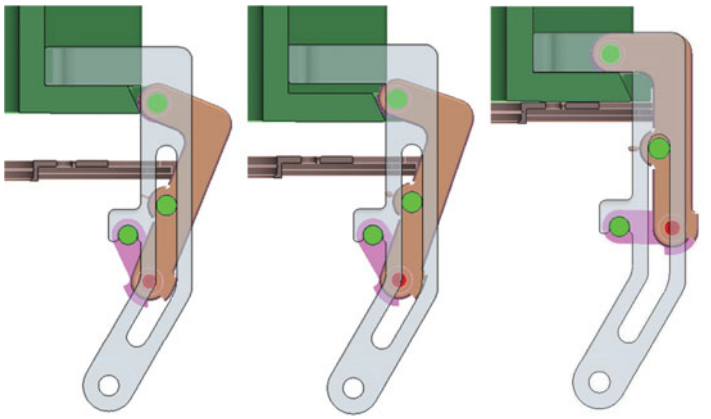

Fig. 10. Latching process.

(2) Actuation apart

The actuation apart is that the latching fingers actuate the grapple fixture to separate from the capture fingers. It is used to realize the functional independency of the capture and latching. The prerequisite of the separation is that the velocity of the capture finger v_{CF} is less than that of the grapple fixture v_{GF} which is substituted with the projection of the velocity of the point T on the z-axis. To obtain the velocity of the point T, some auxiliary lines are added, as shown in Fig. 11. The line JK is parallel to the inclined plane of the interface plate and perpendicular to the line TK at point K. The separation condition is given by

$$\left.\begin{array}{l} v_{\mathrm{CF}} < v_{\mathrm{GF}} \\ \left\{\begin{array}{l} v_{\mathrm{CF}} = \dot{s} \\ v_{\mathrm{GF}} = v_{Tz} \end{array}\right. \end{array}\right\} \Rightarrow \dot{s} < \dot{\varphi}_{21}\sqrt{(L_{JD}\cos(\gamma+\delta+\theta_L))^2 + (L_{JD}\sin(\gamma+\delta+\theta_L) - r)^2}\cos(\delta+\theta_T), \tag{39}$$

where $\begin{array}{l} \theta_T = \arctan\left(\frac{r - L_{JD}\sin(\gamma+\delta+\theta_L)}{L_{JD}\cos(\gamma+\delta+\theta_L)}\right) \\ L_{JD} = \sqrt{(L_{DE} - L_{BJ}\sin\beta_0)^2 + (L_{BE} - L_{BJ}\cos\beta_0)^2} \end{array}$.

(3) Latching dimension

In the rigidizing state, the flexible element produces a preload deformation. The dimensional correlation among the latching finger, latching roller and interface plate is given by

$$(L_{BE} - L_{JB}\cos\beta_0) - g < r + h_{\mathrm{T}}. \tag{40}$$

(4) Capture force and latching force

During each phase, the force analysis of the linkage mechanism is shown in Fig. 11. It shows that the capture fingers independently interact with the grapple fixture during the capture, dragging and linkage phase, the acting force F_G can be regarded as a capture force. During the latching phase, the latching fingers independently interact with the grapple fixture, the acting force F_{LR} can be regarded as a latching force. The two forces are independent each other, i.e., the capture and the latching functions are independent each other.

During the latching phase, the dynamic equation of the capture finger is

$$\left.\begin{array}{l} \sum X = 0 \\ \sum Z = m_{\mathrm{C}}\ddot{s} \end{array}\right\} \Rightarrow F_N - N_L(\sin(\alpha+\gamma) - \mu_1\cos(\alpha+\gamma)) = m_{\mathrm{C}}\ddot{s}, \tag{41}$$

https://doi.org/10.1017/S0263574715000302 Published online by Cambridge University Press

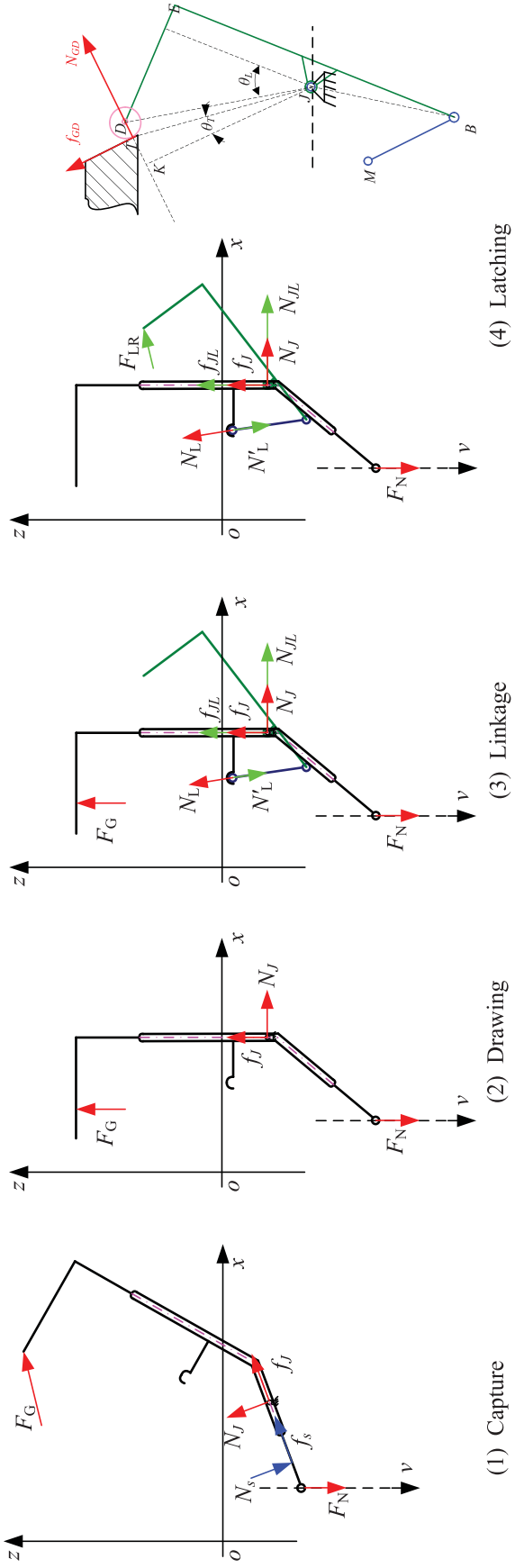

Fig. 11. Force analysis of the linkage mechanism.

https://doi.org/10.1017/S0263574715000302 Published online by Cambridge University Press

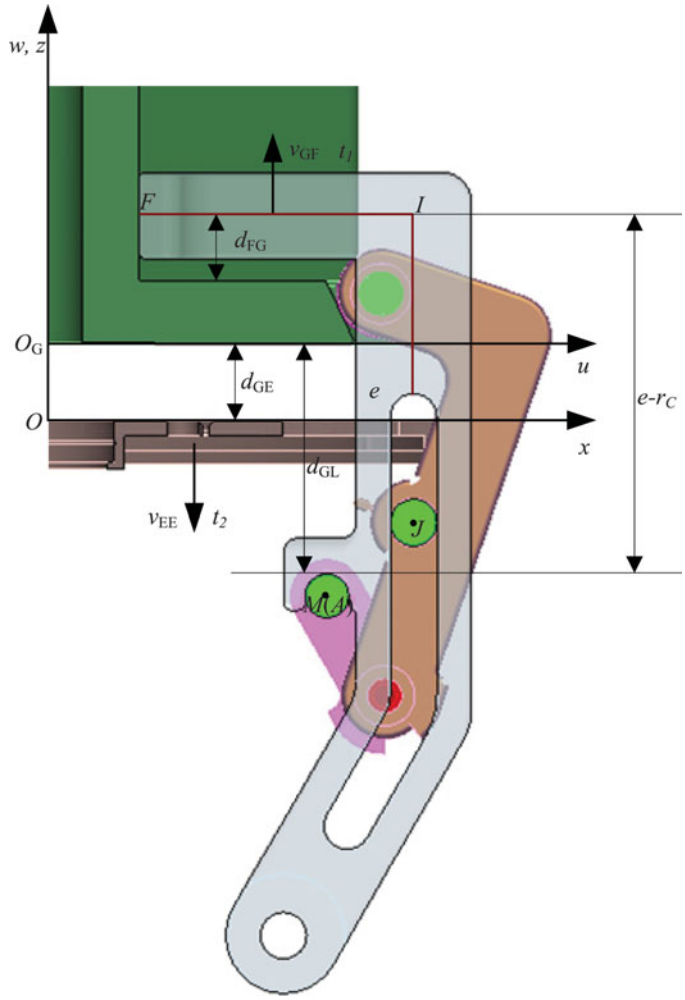

Fig. 12. Relationship among components during release.

where $f_J = \mu_1 N_J$.

The latching force F_{LR} is resolved into a normal force N_{GD} and a tangential force f_{GD} (Fig. 11). The forces N_L and N_L' are a pair of acting force and reacting force. The dynamic equation of the latching mechanism is

$$\begin{aligned} &\sum M_{\mathrm{L}J} = J_{\mathrm{L}J}\ddot{\varphi}_{21} \Rightarrow \\ &N_L' * L_{BJ} \sin(\alpha - \beta_0) - (\mu_2 - 1) N_{GD} * L_{DJ} \cos(\delta + \gamma + \theta_L) - r\mu_2 N_{GD} = J_{\mathrm{L}J}\ddot{\varphi}_{21} \end{aligned}, \tag{42}$$

where $f_{GD} = \mu_2 N_{GD}$.

3.5. Relationship during release phase

The release phase is the inverse process of the capture operation. During the phase, the capture fingers stretch out and deploy with a release speed. The spring-damper system can separate the end-effector from the fixed grapple fixture with a limited distance so that the distance d_{GE} is not long enough for the stretch and deployment of the linking hook. To avoid an impact between the linking hook and the interface plate, an axial separate velocity of the end-effector with respect to the grapple fixture is required and performed by the manipulator. It comes with the release speed of the capture finger. As shown in Fig. 12, the fixed grapple fixture acts as a datum. The relationships are presented as follows.

Presume at the time t, the release displacement S_N of the capture finger is

$$S_N = v_{\mathrm{CF}} t. \tag{43}$$

https://doi.org/10.1017/S0263574715000302 Published online by Cambridge University Press

The release of the lathing fingers is the first release phase during which the end-effector should be static. Therefore, the distance S_N is equal to the distance d_{GE3}, the distance d_{GE} is zero. The corresponding time t_1 is

$$t_1 = d_{GE3}/v_{CF}. \tag{44}$$

The separate velocity v_{EE} happens after the deployment of the latching fingers. Presume the initial time is $t_2(t_2 \geq t_1)$, the distance d_{GE} is

$$d_{GE} = v_{EE}\,(t - t_2)\,, \tag{45}$$

where $t > t_2$. And the distance d_{FG} between the capture finger and the grapple fixture is

$$d_{FG} = S_N - d_{GE}. \tag{46}$$

To avoid a force from being produced between the capture finger and the interface plate, distances d_{FG} is positive, which is expressed as

$$d_{FG} > 0. \tag{47}$$

Any time, the correlation between the two distances d_{FG} and d_{GL} is

$$d_{GL} = e - r_C - h_T - d_{FG}. \tag{48}$$

To avoid the linking hooks from impacting the interface plate, the distance $(d_{GE} - r_C)$ is greater than the maximum pike of the point A, which is written as

$$d_{GE} \geq (z_A)_{max} + r_C. \tag{49}$$

Equation (49) will be stringently constrained in the next section.

Presume the separate velocity v_{EE} is very small or the separate time is very short so that when the distance d_{GL} is equal to zero, the distance d_{GE} just meets Eq. (44). The critical condition is described by

$$\begin{cases} d_{FG} = e - r_C - h_T \\ d_{GE} \geq (z_A)_{max} + r_C \end{cases}. \tag{50}$$

Equation (50) suggests that there is a lot of choices for the separate velocity v_{EE}. For example, it can occur when the distance d_{GL} is nearly equal to zero and the capture finger stops, which is a time-consuming. The best way is that the separate velocity v_{EE} follows the release velocity v_{CF} after the latching release phase.

Thus, the relationships of the mechanical linking process make the capture operation definite. The middle process linking makes the capture and latching functionality independence. Accordingly, the capture force and the latching force are independent of one another. For release, a separation velocity of the end-effector comes with the release speed of the capture fingers. In addition, the functionality independence would make the end-effector achieve large capture misalignment envelope which will be presented in the next section.

4. Model Capture Misalignment Envelope Analysis and Simulation

According to the relativity, the capture misalignment envelope of the end-effector can be defined as the motion range of the grapple fixture within the boundary of the three capture fingers. It contains the positioning error of the end of the manipulator and determines the on-orbit capture capability of the manipulator. Therefore, the capture misalignment envelope of the end-effector is analyzed and simulated as follows.

https://doi.org/10.1017/S0263574715000302 Published online by Cambridge University Press

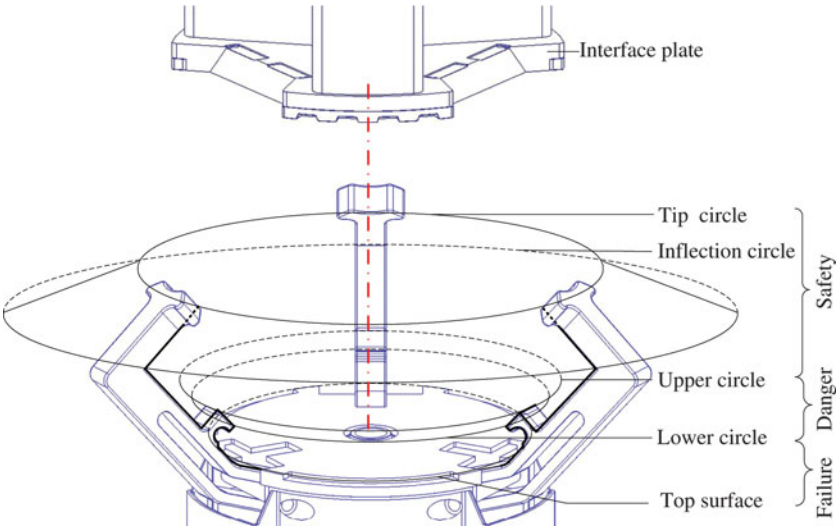

Fig. 13. Enveloping boundary and the interface plate.

4.1. Capture misalignment envelope analysis

The definition aforementioned illustrates the initial states of the end-effector and the grapple fixture, as shown in Fig. 13. The end-effector is fixed. Its three capture fingers begin in the maximal deployed state and form an enveloping boundary. The grapple fixture is within the boundary. Their coordinates align with an offset in the z direction. The grapple fixture moves along or rotates around the coordinate axis so that the range of each misalignment variable can be analyzed independently. Its upper limit and lower limit are determined by the boundary. Presume that the boundary has a tip circle, an inflectional circle, a lower and an upper circle in a turn.

(1) Positional and angular misalignments in the *XOY* plane

In the *XOY* plane, the positional misalignments are dx and dy, the angular misalignment is $d\varphi$(roll). The initial state of the grapple fixture is projected on the *XOY* plane, as shown Fig. 14. The plane OF_iI_i $(i = 1, 2, 3)$ is the plane of symmetry of the capture finger i $(i = 1, 2, 3)$ and the capture feature space i $(i = 1, 2, 3)$. The points A_i, B_i, C_i and $D_i (i = 1, 2, 3)$ are the boundary points of the capture feature space i $(i = 1, 2, 3)$. In the dexterous robot hand such as Metahand and metamorphic anthropomorphic hand, a finger-operation plane and its normal are used to analyze the workspace of the fingers and the orientation and pose of the hand.[51,52] Therefore, the finger plane is a key factor in the misalignment analysis.

There are four criterions for analysis. First, the boundary points A_i and B_i (i = 1, 2, 3) must distribute the two sides of the plane OF_iI_i $(i = 1, 2, 3)$, which ensures that the capture finger is forever within the capture feature space. Second, the interface plate i $(i = 1, 2, 3)$ must be within the planar enveloping boundary of the capture finger i $(i = 1, 2, 3)$, which ensures that the capture finger hook can always enter the capture feature space. Third, the cover of the grapple fixture must be above the boundary of the three capture fingers, which complements the second criterion. Finally, the interface plate must be between the linking hooks and the capture finger hooks, which ensures that the linking hooks can slide inside of the end-effector.

(a) Positional misalignment dy

The positional misalignment dy is the translation distance of the grapple fixture in the y direction. Therefore, a serial of auxiliary lines through the points A_i, B_i, F_i and I_i $(i = 1, 2, 3)$ are added parallel to the y-axis. Some lines intersect both the plane OF_iI_i $(i = 1, 2, 3)$ and the wedge surfaces A_iD_i, B_iC_i $(i = 1, 2, 3)$. Between them the line segments are the translation distances of the grapple fixture. Among them, the minimum value is the positional misalignment dy. The translation of the grapple fixture along the y-axis is symmetrical. There are two distances dy_1 and dy_2.

https://doi.org/10.1017/S0263574715000302 Published online by Cambridge University Press

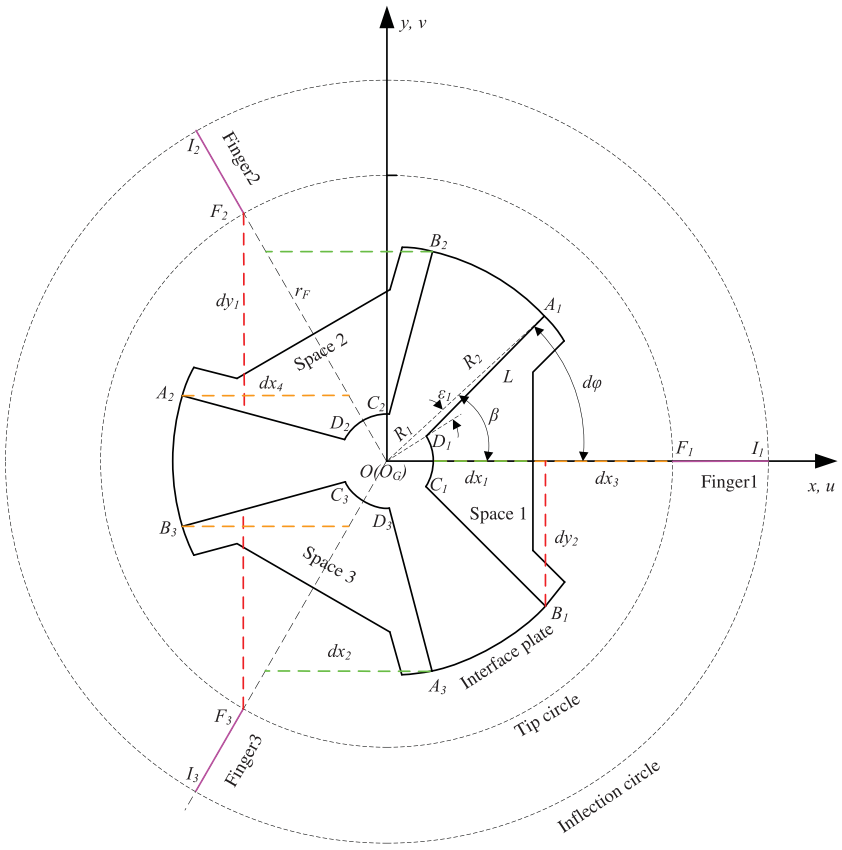

Fig. 14. Analytic schematic of the misalignments (dx, dx and $d\varphi$) in XOY plane.

In spaces 2 and 3, the distance dy_1 is the maximal translation displacement of the grapple fixture before the wedge surface A_2D_2 or B_3C_3 impacts the capture finger 2 or 3. And it is given by

$$dy_1 = r_F \cos 30^\circ - R_2 \sin(60^\circ - \beta) + \frac{R_2 \sin(60^\circ - \beta) - R_1 \sin(60^\circ - \beta + \varepsilon)}{R_2 \cos(60^\circ - \beta) - R_1 \cos(60^\circ - \beta + \varepsilon)} \left(R_2 \cos(60^\circ - \beta) - r_F \sin 30\right), \quad (51)$$

where $\varepsilon = \arccos\left(\frac{R_1^2 + R_2^2 - L^2}{2R_1R_2}\right)$.

In space 1, the distance dy_2 is the maximal translation displacement of the grapple fixture and the boundary point B_1 is in the capture finger plane OF_1I_1. It is a critical condition to meet criterion 1 and given by

$$dy_2 = R_2 \sin\beta. \quad (52)$$

By comparison, the minimum value is dy_2. Therefore, the positional misalignment dy is

$$-R_2 \sin\beta \le dy \le R_2 \sin\beta. \quad (53)$$

(b) Positional misalignment dx

The positional misalignment dx is the translation distance of the grapple fixture along the x-axis. Similarly, a serial of auxiliary lines through the points A_i, B_i, F_i and I_i ($i = 1, 2, 3$) are added parallel to the x-axis. Some lines intersect both the plane OF_iI_i ($i = 1, 2, 3$) and the wedge surfaces A_iD_i, B_iC_i ($i = 1, 2, 3$). A line through the point F_1 intersects both the cylindrical surface C_1D_1 and the hemline 1. These line segments are the translation distances of the grapple fixture. Among them, the minimum value is the positional misalignment dx. The translation of

https://doi.org/10.1017/S0263574715000302 Published online by Cambridge University Press

the grapple fixture along the x-axis is not symmetrical. There are two distances dx_1 and dx_2 along the negative x-axis, and two distances dx_3 and dx_4 along the positive x-axis.

- Distances dx_1 and dx_2 along the negative x-axis

  In space 1, the distance dx_1 is the maximal translation displacement of the grapple fixture. And the hemline 1 of the interface plate intersects the planar enveloping boundary of the capture finger 1 at the point F_1. It is a critical condition to meet criterion 2 and given by

$$dx_1 = d_1 - R_1. \tag{54}$$

  In spaces 2 and 3, the distance dx_2 is the maximal translation displacement of the grapple fixture. And the boundary points B_2 and A_3 are in the capture finger planes OF_2I_2 and OF_3I_3, respectively. It is a critical condition to meet criterion 1 and given by

$$dx_2 = \frac{2}{\sqrt{3}} R_2 \sin\beta. \tag{55}$$

  By comparison, the minimum value is dx_2. Therefore, the low limit of the positional misalignment dx is

$$(dx)_{\text{lm}} = -\min\{dx_1, dx_2\} = -dx_2. \tag{56}$$

- Distances dx_3 and dx_4 along the positive x-axis

  In space 1, the distance dx_3 is the maximal translation displacement of the grapple fixture before the cylindrical surface D_1C_1 impacts capture finger 1. And it is given by

$$dx_3 = r_F - R_1. \tag{57}$$

  In spaces 2 and 3, the distance dx_4 is the maximal translation displacement of the grapple fixture. And the boundary points A_2 and B_3 are in the capture finger planes OF_2I_2 and OF_3I_3, respectively. It is a critical condition to meet criterion 1 given by

$$dx_4 = \frac{2}{\sqrt{3}} R_2 \sin\beta. \tag{58}$$

  By comparison, the minimum value is dx_4. Therefore, the upper limit of the positional misalignment dx is

$$(dx)_{\text{ul}} = \min\{dx_3, dx_4\} = dx_4. \tag{59}$$

  With Eqs. (56) and (59), the positional misalignment dx is

$$-\frac{2}{\sqrt{3}} R_2 \sin\beta \le dx \le \frac{2}{\sqrt{3}} R_2 \sin\beta. \tag{60}$$

(c) Angular misalignment $d\varphi$(roll)

The angular misalignment $d\varphi$ is the rotation angle of the grapple fixture around the z-axis. The rotation is symmetrical. Presume that it is a clockwise rotation. For example, in space 1, the wedge surface A_1D_1 is not the radial plane of the grapple fixture, i.e., the line segment A_1D_1 is not the radius O_GA_1. Thus, it cannot coincide with the plane OF_1I_1 during the rotation. The boundary point D_1 first reaches the plane OF_1I_1, and then point A_1. When the point D_1 reaches, the boundary points A_i and B_i ($i = 1, 2, 3$) still satisfy criterion 1. But when the boundary point A_1 reaches, the boundary points A_i, and B_i ($i = 1, 2, 3$), they are in the critical state of criterion 1, and the angle of rotation is up to the limit of β. Therefore, the angular misalignment $d\varphi$ is

$$-\beta \le d\varphi \le \beta. \tag{61}$$

https://doi.org/10.1017/S0263574715000302 Published online by Cambridge University Press

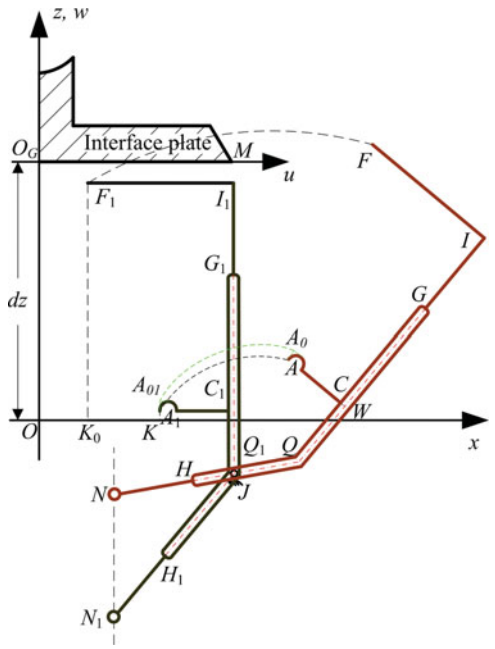

Fig. 15. Analytic schematic of the axial positional misalignment dz.

(2) Positional misalignment dz

The positional misalignment dz is the translation distance of the grapple fixture along the z-axis. Its analysis is based on criterions 2 and 4. The planar enveloping boundary of the capture finger is shown in Fig. 15. The capture finger is in an initial deployment state $ACFIGHN$ and an initial closure centring state $A_1C_1F_1I_1G_1H_1N_1$. The points K_0 and K are the projections of the points F_1 and A_0 on the x-axis, respectively. The boundaries are the line segments FI, IW, WA, A_1K, KK_0 and K_0F_1 and the curves FF_1 and AA_1. Because the curve AA_1 and the linking hook intersect, the curve A_0A_{01} is a substitute. The point A_0 is the intersection point of the linking hook tangents. In UO_GW (XOZ) plane, the mating surface and the incline of the interface plate intersect at the point M which is in the hemline.

The grapple fixture translates along the positive z-axis. When it is at the maximal distance dz_1, the interface plate is outside of the planar enveloping boundary and intersects the curves FF_1 at the point $M_1(d_1, dz_1)$. It is a critical condition to meet criterion 2 and acts as the upper limit. When the grapple fixture is at the minimal distance dz_2, the interface plate is inside of the planar enveloping boundary and intersects the curves A_0A_{01} at the point $M_2(d_1, dz_2)$. It is a critical condition to meet criterion 2 and acts as the lower limit. Therefore, the positional misalignment dz is between the distances dz_2 and dz_1.

With Eq. (6), the maximal distance dz_1 is calculated as

$$\begin{cases} x_{M_1} = d_1 \\ z_{M_1} = d_{z1} \end{cases} \Rightarrow d_{z1} = \begin{pmatrix} -g - (m-n)\cot\phi_{01} + c\cos\phi_{01} + \\ b\cos(\phi_{01} - 30^\circ) + a\sin(\phi_{01} - 30^\circ) \end{pmatrix}, \tag{62}$$

where $\phi_{01} = \arctan\left(\frac{\sqrt{3}a+b}{-a+\sqrt{3}b+2c}\right) + \arcsin\left(\frac{2(d_1-n)}{\sqrt{(-a+\sqrt{3}b+2c)^2+(\sqrt{3}a+b)^2}}\right)$.

Substituting a and b in Eq. (6) with $(d + r_C)$ and $(b–e + r_C)$, respectively. The minimal distance dz_2 is calculated as

$$\begin{cases} x_{M_2} = d_1 \\ z_{M_2} = d_{z2} \end{cases} \Rightarrow d_{z2} = \begin{pmatrix} -g - (m-n)\cot\phi_{02} + c\cos\phi_{02} + \\ (b - e + r_C)\cos(\phi_{02} - 30^\circ) + (d + r_C)\sin(\phi_{02} - 30^\circ) \end{pmatrix}, \tag{63}$$

https://doi.org/10.1017/S0263574715000302 Published online by Cambridge University Press

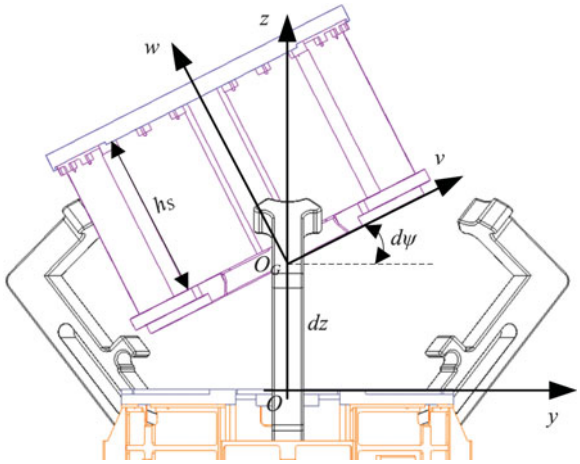

Fig. 16. Analytic schematic of the angular misalignment $d\psi$ (yaw).

where

$$\phi_{02} = \arctan\left(\frac{b+\sqrt{3}d-e+(\sqrt{3}+1)r_C}{\sqrt{3}b+2c-d-\sqrt{3}e+(\sqrt{3}-1)r_C}\right) + \arcsin\left(\frac{2\,(d_1-n)}{\sqrt{(\sqrt{3}b+2c-d-\sqrt{3}e+(\sqrt{3}-1)r_C)^2+(b+\sqrt{3}d-e+(\sqrt{3}+1)r_C)^2}}\right).$$

Therefore, the positional misalignment dz is

$$d_{z2} \le dz \le d_{z1}. \tag{64}$$

It ensures that the interface plate is always between the capture finger hook and the linking hook, which is criterion 4. Equation (64) stringently constrained the release condition in Eq. (49).

(3) Angular misalignment $d\psi$(yaw)
The angular misalignment $d\psi$ is the rotation angle of the grapple fixture around the x-axis. The rotation is symmetrical. Presume that it is a counter-clockwise rotation, as shown in Fig. 16. And presume that the capture finger plane $OF_iI_i(i=1,2,3)$ intersects the corresponding interface plate hemline i $(i=1,2,3)$ at the point P_i $(i=1,2,3)$. During the rotation, the point P_1 is static, while point P_2 ascends and point P_3 descends.
The trajectory of the point $P_i(i=2,3)$ is a line of intersection of the capture finger plane $OF_iI_i(i=2,3)$ and the surface of revolution of the hemline i $(i=2,3)$. It is an elliptic curve expressed as

$$\left(x-\frac{d_1}{4}\right)^2+\frac{3}{8}z^2=\left(\frac{3d_1}{4}\right)^2, \tag{65}$$

where $-\frac{1}{2}d_1 \le x \le -\frac{1}{2}R_1; 0 \le z \le \sqrt{\frac{2}{3}(2d_1+R_1)(d_1-R_1)}$.
The correlation between the angle ψ and the coordinate components x, y and z of the point P_i $(i=2,3)$ is given by

$$\begin{cases}\tan\psi=\frac{z}{y}\ge 0\\ y=-\sqrt{3}x\end{cases} \Rightarrow z=y\tan\psi=-\sqrt{3}x\tan\psi. \tag{66}$$

https://doi.org/10.1017/S0263574715000302 Published online by Cambridge University Press

Substituting Eq. (66) into Eq. (65), we yield a parametric equation as follows:

$$\begin{cases} x_{P_2} = -\dfrac{2d_1 \cos\psi}{(3+\cos\psi)} \\ y_{P_2} = \dfrac{2\sqrt{3}d_1 \cos\psi}{(3+\cos\psi)} \\ z_{P_2} = \dfrac{2\sqrt{3}d_1 \sin\psi}{(3+\cos\psi)} \end{cases}. \tag{67}$$

With the domain x in Eq. (65), the range of the angle ψ is calculated as

$$0 \le \psi \le \arccos\left(\frac{3R_1}{4d_1 - R_1}\right). \tag{68}$$

In addition, the range of the angle ψ can be further constrained by criterions 2 and 3 as follows. In space 2, the interface plate must be within the enveloping boundary of capture finger 2. Therefore, the point $P_2(x_{P2}, z_{P2})$ is below the corresponding boundary curve point $F_{21}(x_{P2} = x_{F21}, z_{F21})$, which is expressed as

$$\begin{cases} x_{P_2} = x_{F_{21}} \\ z_{P_2} \le z_{F_{21}} \end{cases} \Rightarrow dz + \frac{2\sqrt{3}d_1 \sin\psi}{(3+\cos\psi)} \le \begin{pmatrix} -g - (m-n)\cot\phi_{03} + c\cos\phi_{03} + \\ b\cos(\phi_{03} - 30^\circ) + a\sin(\phi_{03} - 30^\circ) \end{pmatrix}, \tag{69}$$

where $\phi_{03} = \arctan\left(\frac{\sqrt{3}a+b}{-a+\sqrt{3}b+2c}\right) + \arcsin\left(\frac{2\left(\frac{4d_1\cos\psi}{(3+\cos\psi)} - n\right)}{\sqrt{(-a+\sqrt{3}b+2c)^2+(\sqrt{3}a+b)^2}}\right)$.

In space 3, point P_3 is undoubtedly below point P_2. It satisfies the upper limit of criterion 2 according to the analysis of the positional misalignment dz. To meet the lower limit, point $P_3(x_{P3}, z_{P3})$ must be above the corresponding boundary curve point $A_{031}(x_{P3} = x_{A031}, z_{A031})$, which is written as

$$\begin{cases} x_{P_3} = x_{A_{031}} \\ z_{P_3} \ge z_{A_{031}} \end{cases} \Rightarrow dz - \frac{2\sqrt{3}d_1 \sin\psi}{(3+\cos\psi)} \ge \begin{pmatrix} -g - (m-n)\cot\phi_{04} + c\cos\phi_{04} \\ + (b - e + r_C)\cos(\phi_{04} - 30^\circ) + (d + r_C)\sin(\phi_{04} - 30^\circ) \end{pmatrix}, \tag{70}$$

where $\phi_{04} = \arctan\left(\frac{\sqrt{3}a+b}{-a+\sqrt{3}b+2c}\right) + \arcsin\left(\frac{2\left(\frac{4d_1\cos\psi}{(3+\cos\psi)} - n\right)}{\sqrt{(-a+\sqrt{3}b+2c)^2+(\sqrt{3}a+b)^2}}\right)$.

In space 3, the cover of the grapple fixture descends with the rotation and has the lowest point. To make criterion 3 be tenable, the cover of the grapple fixture is above the highest point of the planar enveloping boundary of capture finger 3. It is described by

$$dz + (h_S + h_T)\cos\psi - R_2 \sin\psi \ge \left(z_{F_3}\right)_{\max}. \tag{71}$$

Presume that $\psi_{\min}$ is the minimum value among the solutions to Eqs. (68)–(71), the angular misalignment $d\psi$ is

$$-\psi_{\min} \le \mathrm{d}\psi \le \psi_{\min}. \tag{72}$$

(4) Angular misalignment $d\theta$(Pitch)
The angular misalignment $d\theta$ is the rotation angle of the grapple fixture around the y-axis. The rotation is not symmetrical and the constraint conditions change with the direction of rotation as follows.

(a) Clockwise rotation
In space 1, Fig. 17 shows that point P_1 ascends and its trajectory is a circular curve expressed as

$$x^2 + z^2 = d_1^2, \tag{73}$$

where $0 < x \le d_1$, $0 \le z < d_1$.

https://doi.org/10.1017/S0263574715000302 Published online by Cambridge University Press

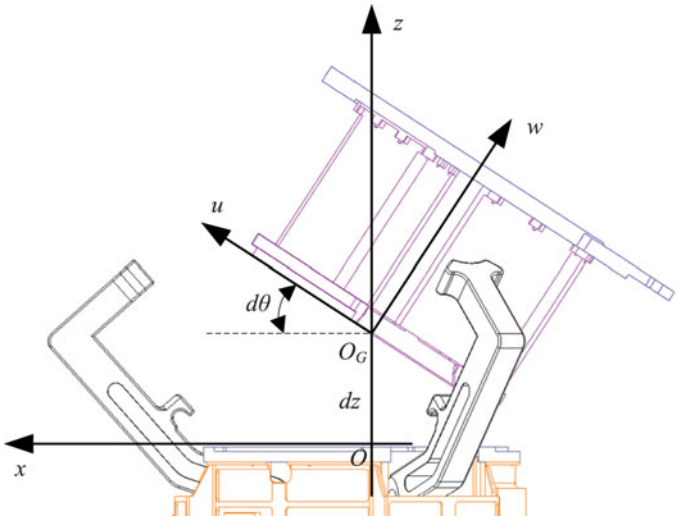

Fig. 17. Analytic schematic of the angular misalignment $d\theta$ (pitch).

To satisfy criterion 2, the point $P_1(x_{P1}, z_{P1})$ must be below the corresponding boundary curve point $F_{11}(x_{P1} = x_{F11}, z_{F11})$, which is written as

$$\begin{cases} x_{P_1} = x_{F_{11}} \\ z_{P_1} \le z_{F_{11}} \end{cases} \Rightarrow dz + d_1 \sin\theta \le \begin{pmatrix} -g - (m-n)\cot\phi_{05} + c\cos\phi_{05} + \\ b\cos(\phi_{05} - 30^\circ) + a\sin(\phi_{05} - 30^\circ) \end{pmatrix}, \tag{74}$$

where $\phi_{05} = \arctan\left(\frac{\sqrt{3}a+b}{-a+\sqrt{3}b+2c}\right) + \arcsin\left(\frac{2(d_1\cos\theta - n)}{\sqrt{(-a+\sqrt{3}b+2c)^2+(\sqrt{3}a+b)^2}}\right)$.
In space 2 and 3, the trajectory of point P_i $(i = 2, 3)$ is a hyperbolic curve expressed as

$$\left(x + \frac{3}{4}d_1\right)^2 - \frac{1}{8}z^2 = \frac{1}{16}d_1^2, \tag{75}$$

where $-d_1/2 \le \mathrm{x} \le -R_1/2$, $0 \le z$.
The correlation between the angle θ and the coordinate components x, y and z of point P_i $(i = 2, 3)$ is given by

$$\begin{cases} \tan\psi = \frac{z}{-x} \ge 0 \Rightarrow z = -x\tan\psi \\ y = -\sqrt{3}x \end{cases}. \tag{76}$$

Substituting Eq. (76) into Eq. (75), Eq. (75) becomes a parametric equation as follows:

$$\begin{cases} x_{P_2} = -\dfrac{2d_1\cos\theta}{1+3\cos\theta} \\ y_{P_2} = \dfrac{2\sqrt{3}d_1\cos\theta}{1+3\cos\theta} \\ z_{P_2} = \dfrac{2d_1\sin\theta}{1+3\cos\theta} \end{cases}. \tag{77}$$

With the range of x in Eq. (75), the range of the angle θ is calculated as

$$0 \le \theta \le \arccos\left(\frac{\frac{1}{2}d_1 - \frac{1}{2\sqrt{3}}l}{\frac{1}{2}d_1 + \frac{\sqrt{3}}{2}l}\right). \tag{78}$$

https://doi.org/10.1017/S0263574715000302 Published online by Cambridge University Press

In space 2(or 3), point P_2 descends and is below point P_1. It meets the upper limit of criterion 2 as the analysis of positional misalignment dz. To obtain the lower limit, point $P_2(x_{P2}, z_{P2})$ must be above the corresponding boundary curve point $A_{021}(x_{P2} = x_{A021}, z_{A021})$, which is described by

$$\begin{cases} x_{P_2} = x_{A_{021}} \\ z_{P_2} \geq z_{A_{021}} \end{cases} \Rightarrow dz - \frac{2d_1 \sin\theta}{1 + 3\cos\theta} \geq \begin{pmatrix} -g - (m-n)\cot\phi_{06} + c\cos\phi_{06} + \\ (b - e + r_C)\cos(\phi_{06} - 30^\circ) + (d + r_C)\sin(\phi_{06} - 30^\circ) \end{pmatrix}, \tag{79}$$

where $\phi_{06} = \arctan\left(\frac{\sqrt{3}a+b}{-a+\sqrt{3}b+2c}\right) + \arcsin\left(\frac{2\left(\frac{4d_1\cos\theta}{1+3\cos\theta} - n\right)}{\sqrt{(-a+\sqrt{3}b+2c)^2+(\sqrt{3}a+b)^2}}\right)$.

In space 2(or 3), the cover of the grapple fixture has the lowest point, which must be above the highest point of the planar enveloping boundary of capture finger 2(or 3) in order to satisfy criterion 3. It is given by

$$dz + (h_S + h_T)\cos\theta - R_2\sin\theta \geq \left(z_{F_2}\right)_{\max}. \tag{80}$$

Presume that θ_{lm} is the minimum value among the solutions to Eqs. (74), (78)–(80). It is the lower limit of the angular misalignment $d\theta$ and expressed as

$$(\mathrm{d}\theta)_{\text{lm}} = -\theta_{\text{lm}}. \tag{81}$$

(b) Counter-clockwise rotation

Compared with the clockwise rotation, the counter-clockwise rotation cannot change the trajectory equations, but does change the constraint conditions.

In space 2(or 3), point P_2 ascends. For the satisfaction of criterion 2, the point $P_2(x_{P2}, z_{P2})$ must be below the corresponding boundary curve point $F_{22}(x_{P2} = x_{F22}, z_{F22})$. This condition can be expressed as

$$\begin{cases} x_{P_2} = x_{F_{22}} \\ z_{P_2} \leq z_{F_{22}} \end{cases} \Rightarrow dz + \frac{2d_1 \sin\theta}{1 + 3\cos\theta} \leq \begin{pmatrix} -g - (m-n)\cot\phi_{07} + c\cos\phi_{07} + \\ b\cos(\phi_{07} - 30^\circ) + a\sin(\phi_{07} - 30^\circ) \end{pmatrix}, \tag{82}$$

where $\phi_{07} = \arctan\left(\frac{\sqrt{3}a+b}{-a+\sqrt{3}b+2c}\right) + \arcsin\left(\frac{2\left(\frac{4d_1\cos\theta}{1+3\cos\theta} - n\right)}{\sqrt{(-a+\sqrt{3}b+2c)^2+(\sqrt{3}a+b)^2}}\right)$.

In space 1, point P_1 descends and is below point P_2. It makes the upper limit of criterion 2 be tenable, just as the analysis of positional misalignment dz. To obtain the lower limit, point $P_1(x_{P1}, z_{P1})$ must be above the corresponding boundary curve point $A_{011}(x_{P1} = x_{A011}, z_{A011})$, which is described by

$$\begin{cases} x_{P_1} = x_{A_{011}} \\ z_{P_1} \geq z_{A_{011}} \end{cases} \Rightarrow dz - d_1\sin\theta \geq \begin{pmatrix} -g - (m-n)\cot\phi_{08} + c\cos\phi_{08} + \\ (b - e + r_C)\cos(\phi_{08} - 30^\circ) + (d + r_C)\sin(\phi_{08} - 30^\circ) \end{pmatrix}, \tag{83}$$

where $\phi_{08} = \arctan\left(\frac{\sqrt{3}a+b}{-a+\sqrt{3}b+2c}\right) + \arcsin\left(\frac{2(d_1\cos\theta - n)}{\sqrt{(-a+\sqrt{3}b+2c)^2+(\sqrt{3}a+b)^2}}\right)$.

In space 1, the cover of the grapple fixture descends and has the lowest point. To meet criterion 3, the lowest point is above the highest point of the enveloping boundary of the capture finger. It is written as

$$dz + (h_S + h_T)\cos\theta - R_2\sin\theta \geq \left(z_{F_1}\right)_{\max}. \tag{84}$$

Presume that θ_{um} is the minimum value among the solutions to Eqs. (74), (82)–(84) and it acts as the upper limit of the angular misalignment $d\theta$ and is given by

$$(\mathrm{d}\theta)_{\text{um}} = \theta_{\text{um}}. \tag{85}$$

https://doi.org/10.1017/S0263574715000302 Published online by Cambridge University Press

Table II. Simulation data of the capture misalignment.

	Position/mm			Angle/(°)			
Number	dx	dy	dz	$d\psi$	$d\theta$	$d\varphi$	Result
1	40	0	30	0	0	0	F
2	40	0	40	0	0	0	S
3	−40	40	65	−4	−4	−4	S
4	−40	40	65	4	4	4	S
5	−40	40	65	−4	−4	4	S
6	−40	40	65	4	4	−4	S
7	40	−40	45	4	4	4	F
8	40	−40	65	4	4	4	S
9	40	−40	65	−4	−4	−4	S
10	40	−40	65	4	−4	4	S
11	40	−40	65	−4	4	−4	S
12	−40	−40	65	−4	−4	−4	S
13	−40	−40	65	4	4	4	S
14	−40	−40	65	4	4	−4	S
15	−40	−40	65	−4	−4	4	S
16	40	40	130	4	4	4	S
17	40	40	130	−4	−4	−4	S
18	40	40	130	−4	−4	4	S
19	40	40	130	4	−4	−4	S
20	−40	40	130	−4	−4	−4	S
21	−40	40	130	4	4	4	S
22	−40	40	130	−4	−4	4	S
23	−40	40	130	4	4	−4	S
24	−40	−40	130	−4	−4	−4	S
25	−40	−40	130	4	4	4	S
26	−40	−40	130	4	4	−4	S
27	−40	−40	130	−4	−4	4	S
28	0	0	140	0	0	0	S

S: successful capture operation, F: failed capture operation

With Eqs. (81) and (85), the angular misalignment $d\theta$ is

$$-\theta_{\mathrm{lm}} \leq \mathrm{d}\theta \leq \theta_{\mathrm{um}}. \tag{86}$$

From (1)–(4), it can be concluded that the misalignments dx, dy, dz and $d\varphi$ are independent and have a specific range. However, the angular misalignments $d\psi$ and $d\theta$ are related to dz. The angular misalignment $d\theta$ is also related to the direction of rotation of the grapple fixture. In addition, the angular misalignments $d\psi$, $d\theta$ and $d\varphi$ are in general coupling. Therefore, the real results need simulations and experiments.

4.2. Capture misalignment envelope simulation

In order to achieve the capture misalignment envelope of the end-effector model and simultaneously demonstrate the relationships, a variety of capture operations were simulated with ADAMS software. During the simulation, the end-effector is fixed, the position and orientation of the grapple fixture changed with respect to the coordinate system of the end-effector. After a limited position and orientation is given, the grapple fixture is in a free floating and static state. The capture fingers perform the whole capture operation. The simulation results show that the motion of the mechanical linking corresponds definitely to the capture process, and the capture misalignment envelope meets the requirements. Part of the simulation data and results are shown in Table II. The corresponding analysis is presented as follows.

The data in row no.28 show that when the grapple fixture only moves in the z direction, its positional misalignment dz is up to 140 mm. While the grapple fixture changes both its position and

https://doi.org/10.1017/S0263574715000302 Published online by Cambridge University Press

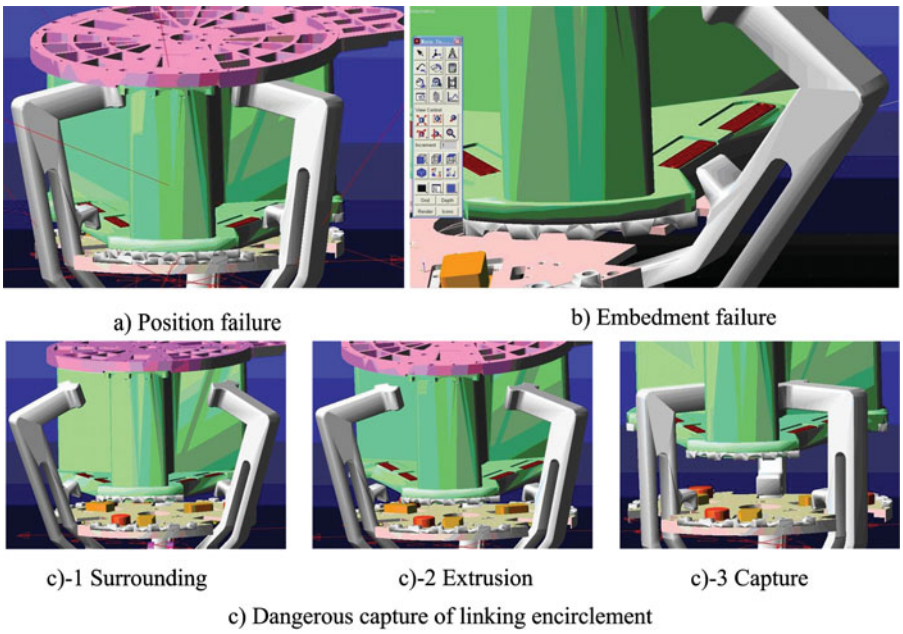

Fig. 18. Capture Failure and danger status.

orientation, the positional misalignment dz is only up to 130 mm. It shows that the misalignment variables are coupling. One increase in some directions means one decrease in the others directions. These values of the misalignments dx, dy, dz, $d\psi$, $d\theta$ and $d\varphi$ can be used to preliminarily evaluate the misalignment envelope of the end-effector. They are also used to direct the position and angle determination during the simulation and experiments.

The data in rows no. 1, 2 and 7 show that the capture operations are failure and danger, as shown in Fig. 18. Their analyses are as follows.

(a) When the grapple fixture is at the position of row no. 1, the failure is that the capture finger hook and the linking hook are simultaneously in the capture feature space. The capture finger hook is used to constrain and drag the interface plate. It should always be above the interface plate. While the linking hook is used to go into the end-effector and drive the latching mechanism, it must be always be below the interface plate. That is, the interface plate must be permanently between the capture finger hook and the linking hook during the capture, which is criterion 4. As a result, the three-finger enveloping space from the linking hook to the tip of the capture finger is for safety, called the safe capture space, as shown in Fig. 13, in which, all the capture operations are performed.

(b) When the grapple fixture is at the position and orientation of row no. 7, the failure is that the linking hook imbeds in the interface plate. In fact, this situation cannot happen because all parts are rigid. It shows that the linking hook is a key factor of the capture operation and the capture misalignment envelope analysis, and it divides the three-finger enveloping space into three segments: failure, danger and safety (Fig. 13).

(c) Compared with the data in row no.1, the data in row no.2 show that the grapple fixture again moves a distance of 10 mm in the z direction. At that position, the interface plate is surrounded by the three linking hooks. Because the grapple fixture is in a free floating state, the linking hooks can press it into the safe capture space. As a result, the capture operation achieves success. However, if the grapple fixture is fixed in the self-relocation and payload handling cases, this situation would cause them to interfere with each other, or even worse the interface plate could be seized up. Therefore, it must be avoided.

The three items demonstrate that the capture operation must be performed in the safe capture space from the opposite point of view.

https://doi.org/10.1017/S0263574715000302 Published online by Cambridge University Press

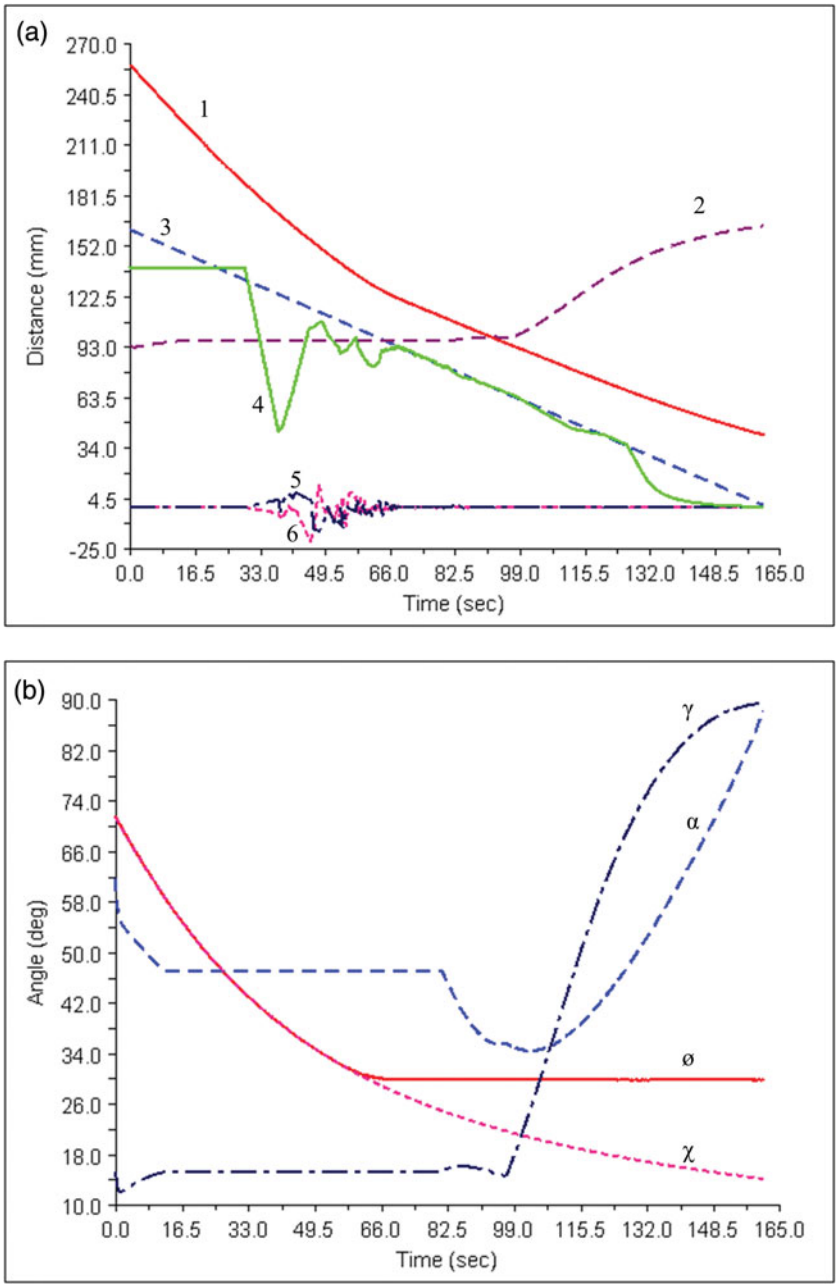

Fig. 19. Position and angle curves of the grapple fixture and the linkage mechanism. (a) Position. (b) Angle.

Figure 19 shows the trajectory curves of the grapple fixture and the linkage mechanism during the capture operation, which is performed when the grapple fixture is at the position of the row no. 28. The analysis is presented as follows.

(1) Positional curve 1 is the trajectory of the capture finger tip (point *F*). Its curvic segment suggests the capture phase and corresponds to capture steps (2) and (3). Its linear segment implies the dragging, linkage and latching phase, and it corresponds to capture steps (4) and (5).
(2) Positional curve 2 tracks the centroid of the link. At the outset of the curve, it changes a little. The reason is that when the capture finger is in the maximal deployed state, it contacts with the linking shaft and causes the link to deploy a little. As the capture finger retracts and closes, the return springs make the link back to its initial position and keep static. Accordingly, the curve becomes horizontal. Then the curve changes a little again, and suggests that the linking hook

https://doi.org/10.1017/S0263574715000302 Published online by Cambridge University Press

engages the linking shaft and drives the links to mate with the latching fingers. The latching mechanism is actuated by the linking hook to rotate as a whole until the links depart from the latching fingers. Subsequently, the linking hook actuates the linking shaft to move, and the links drive the latching fingers rotation till to the end, which is identical with the curvic segment. The point of intersection of positional curves 1 and 2 suggests the beginning of the linking.

(3) Positional curves 3, 4 and 5 illustrate the change of the positional misalignments dx, dy and dz of the grapple fixture, respectively. They have only one considerable fluctuation, especially curve 5. It shows that the spring-damper systems can effectively prevent the grapple fixture from impact/rebound and make the docking soft. The final curvic segment of curve 5 shows that the grapple fixture is actuated by the latching fingers. The slope of its ascending segment is much greater than that of the linear segment which coincides with line 6. It shows that the velocity of the grapple fixture is greater than that of the capture finger and they separate at the initial point of the ascending segment. Its ascending segment corresponds to the drag and mating process. Its horizontal segment suggests the latching preload course.
(4) Positional line 6 is the trajectory of the nut or point N.
(5) Angular curves Φ and χ illustrate the motion of the capture finger. They are consistent with positional curve 1. Their coincident segment shows that the capture finger slides along the deployment/closure segment and performs capture. Their separation point implies that the guide pin is at the initial position of the transition segment. It shows that the transition segment is very short and the simplification in Section 3 is reasonable. After the separation, the angle Φ curve becomes horizontal and its value is equal to 30°, while the angle χ curve decreases with the motion of the capture finger.
(6) Angular curve α illustrates the motion of the link, and it is in accordance with positional curve 2. In its initial segment, the link is back to its initial position. In its horizontal segment, the link is static. In its descending segment, the link is actuated by the linking hook to engage with the latching finger. In its bottom segment, the linking hook still drives the link and the latching finger to rotate together, till the link is parallel to the axis of the end-effector. In its ascending segment, the link and the latching finger separate, and the link actuates the latching finger rotation. The final value of the angle α is less than 90°, which is used to ensure the secure latching for the errors existing in the assembly.
(7) Angular curve γ illustrates the motion of the latching finger, and it agrees with the angular curve α. Similarly, there is a little change at its beginning. The horizontal segment shows that the latching fingers are static. The final value of the angle γ is equal to 90°, which is used for complete rigidization.

The simulation data and curves demonstrate that the mechanical linking and the middle process linking used in the end-effector are effective, and the capture misalignment envelope of the end-effector meets the requirements. However, the simulation should be verified by experiments.

5. Prototype and Experiment for the Misalignment Envelope Calibration, and Self-relocation Capture and Payload Handling

The engineering prototypes were built, including a seven DOF manipulator. With them, two experiments were performed to confirm the characteristics of the end-effector and their suitability for self-relocation and payload handling of the manipulator. They are presented as follows.

5.1. Misalignment envelope calibration

The capture misalignment envelope of the end-effector was calibrated on a semi-physical simulation testbed system, as shown in Fig. 20. The system contains two six DOF industrial robot arm systems and laser tracker API. The end-effector is attached to the end of the right robot arm. The grapple fixture is mounted on a force moment sensor on the end of the left robot arm. One of their engagement positions is selected as a datum which is calibrated by the laser tracker. Then the end-effector is static at the datum and the right robot arm becomes rigid. Its capture fingers are in a maximal deployed state. The grapple fixture side is movable. After the left robot arm positions the grapple fixture to a given position with respect to the datum, it switches to a compliance control mode. The whole capture operation is performed by the capture fingers, and the grapple fixture side follows. During the release,

https://doi.org/10.1017/S0263574715000302 Published online by Cambridge University Press

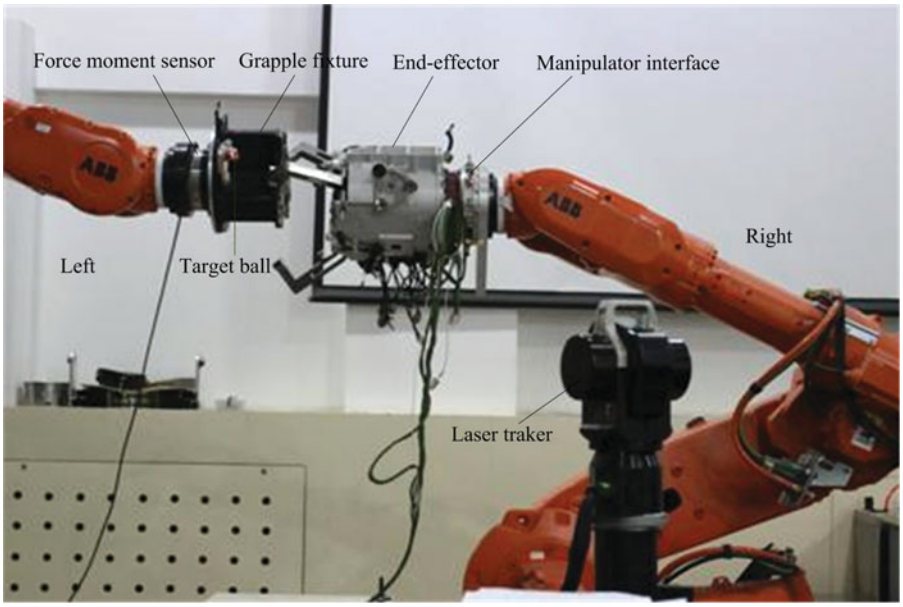

Fig. 20. Experimental system of the end-effector capture misalignment measure.

the grapple fixture separates from the end-effector with an axial velocity, which follows the release speed of the capture fingers stretch and deployment. Based on the simulation, a serial of positions are tested. The testing results are more excellent than the simulation results. Part of the testing data is shown in Table III. The comparison with Table II and analysis are presented as follows.

(1) The positional misalignments *dx*, *dy* and *dz* influence one another. Compared with the data row of no. 1 in Table III with those of row no. 28 in Table II, they both have only the positional misalignment *dz*, and the former is a little greater than the latter. Comparing position (−45 mm, 50 mm, 144 mm, 0°, 0°, 0°) with position (−45.8 mm, 50.0 mm, 148.1 mm, 0°, 0°, 0°) of row no. 4 in Table III, when the grapple fixture is at the former position, the simulation shows that the grapple fixture floats away as one capture finger impacts it during capture. It suggests that if the grapple fixture is in a free floating and static state, the best way of capture is that the three capture fingers simultaneously contact the grapple fixture. On the contrary, when the grapple fixture is at the latter position, the testing shows that the capture is a success without any abnormity. Comparing the data of row no. 1 with row no. 4 rows in Table III, it shows that the positional misalignment *dx* and *dy* are both greater than 40 mm while their *dz* is the same. Comparing the data of row no. 28 row in Table II with the former position, it shows that as the other two positional misalignments *dx* and *dy* increase, the simulation results show that the value of *dz* obviously decreases. Comparing the data of row no. 4 with those of row no. 5 in Table III, it shows that when the positional misalignment *dy* is −43.1 mm, the absolute value of *dx* is greater than 70 mm and the value of *dz* decreases 3.9 mm.

(2) As the angular misalignments increase, the positional misalignments decrease slightly. Comparing the data of the rows no. 13, 17–18, 21–22, 24–25, and 30–31 in Table III with those of any row in Table II, the former is greater than the latter. The testing results also show that if the positional misalignments decrease a little, the angular misalignments increase notably, particularly the angular misalignment $d\theta$(roll). During the testing, the grapple fixture is constrained by the left robot arm which is fixed, which can be imagined as the grapple fixture is constrained by a six DOF spring attached to the base. This capture is also called constraint capture. As for the capture of the constraint object, if one capture finger grapples the grapple fixture, the capture is a success. Compared with the data in Table II, the data in Table III shows that the constraint capture enlarges the capture misalignment envelope of the end-effector. As a result, the capture misalignment envelope of the end-effector meets the requirements of both the free floating target capture and the constraint target capture.

https://doi.org/10.1017/S0263574715000302 Published online by Cambridge University Press

Table III. Testing data of the capture misalignment envelope.

	Position/mm			Angle/(°)			
Number	dx	dy	dz	$d\psi$	$d\theta$	$d\varphi$	Result
1	−1.1	−0.1	148.1	0.0	0.0	0.0	S
2	40.4	41.3	106.0	0	0	0	S
3	−40.5	41.4	129.2	0	0	0	S
4	−45.8	50.0	148.1	0.0	0.0	0.0	S
5	−71.1	−43.1	144.2	0.0	0.0	0.0	S
6	−12.0	−21.5	135.1	−5.7	7.7	−16.7	S
7	63.5	−26.0	126.4	2.8	13.8	−0.72	S
8	20.9	37.4	134.7	−2.9	3.1	−22.6	S
9	26.7	−55.3	143.0	10.5	3.1	5.2	S
10	71.9	−21.6	133.4	3.8	7.9	0.5	S
11	9.8	10.9	118.0	9.0	3.9	30.0	S
12	32.0	23.7	112.3	9.2	5.5	28.4	S
13	49.9	−71.7	147.0	7.0	8.5	7.9	S
14	33.7	27.55	152.0	1.8	4.8	5.6	S
15	47.9	78.9	129.3	1.6	4.9	3.4	S
16	−11.0	−53.9	131.1	−12.4	−4.6	12.5	S
17	−59.6	−40.7	130.7	−12.4	−4.6	12.5	S
18	−59.9	−40.7	130.7	−9.2	−9.3	−12.0	S
19	24.4	−28.3	131.5	−9.2	−9.2	−12.0	S
20	−23.1	35.9	131.3	−9.2	−9.2	−12.0	S
21	−66.2	47.7	130.8	−9.2	−9.2	−12.0	S
22	−75.1	−6.4	133.6	−9.2	−9.2	−12.0	S
23	−65.6	−62.5	133.4	−9.2	−9.2	−12.0	F
24	−66.5	−61.6	123.7	−9.2	−9.2	−12. 1	S
25	50.7	35.5	154. 3	6.2	6.1	−11.0	S
26	46.2	53.7	117.9	7.6	3.9	7.1	S
27	42.9	41.6	127.8	7.5	4.0	5.9	S
28	−44.4	59.0	126.9	7.4	4.2	4.3	S
29	−73.6	−48.4	126.0	7.4	4.2	4.3	S
30	−73.7	−48.5	134.9	7.4	4.2	4.3	S
31	65.9	−87.0	136.6	7.4	4.2	4.4	S

S: successful capture operation; F: failed capture operation

(3) As for the failure capture, the simulation illustrates it from the point view of the linking hook, while the testing does it from the point view of the capture finger hook. During the simulation, the capture operation is outside of the safe capture space. But during the testing, the interface plate of the grapple fixture is inside of the safe capture space, and its failure is that the capture finger tip trough is constrained by the edge of the wedge, as shown in Fig. 21. From the point of view of the analysis criterions in Section 4.1, the failure reason is that the boundary points of the capture feature space distributes one side of the capture finger plane. It is against the analysis criterion 1. The failure capture demonstrates that the analysis criterions and methods are effective for the end-effector.

(4) As for the soft capture, the free floating state of the grapple fixture in the simulation suggests an absolute compliance and it leads to the success of the danger capture operation. While the soft docking is illustrated in Fig. 19 and the corresponding analysis. During the testing, the soft capture is achieved by the compliance motion of the left robot arm. The testing results of the capture operation are shown in Fig. 22 when the grapple fixture is at the position of row no. 2 in Table III. The position curve of the nut shows that the capture velocity is smaller than the release velocity which changes a little at the transition segment. For OOS, The suitable increase of the release velocity is valuable for the decrease of the working hours and working pressure.

https://doi.org/10.1017/S0263574715000302 Published online by Cambridge University Press

Fig. 21. Interference failure capture.

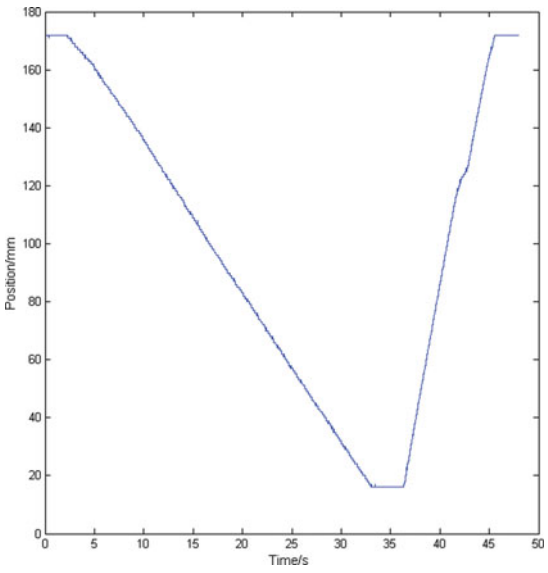

Fig. 22. Nut position curve.

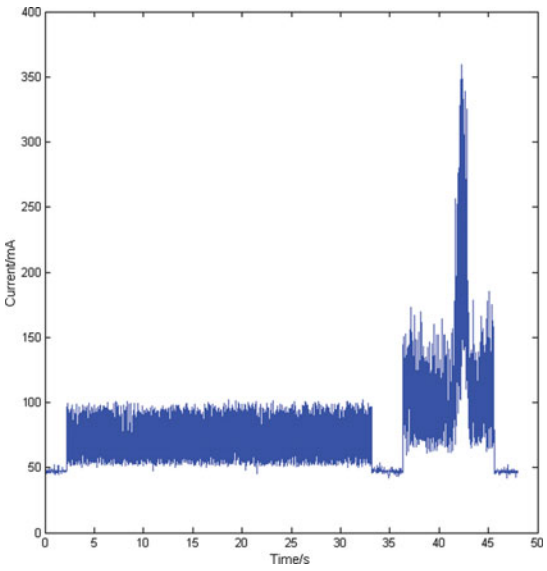

Fig. 23. Motor current curve.

Figure 23 illustrates the change of the motor current. The maximum instant current is about 350 mA. The stop current is about 47 mA, the capture current is about 70 mA, and the release current is about 105mA.

Figure 24 illustrates the corresponding force and moment. The forces in X, Y and Z direction are smaller than 15 N, 8 N and 40 N, respectively. The moments T_x and T_y are small, but the moment T_z increases greatly when the time is 64 s. The reason is that the compliance control of the left robot arm is limited. During the capture operation testing, the industrial robot arm vibrated and the grapple fixture moved back and forth in the boundary of the capture fingers. All the forces and moments have the same vibration and abrupt-change phenomena. However, their steady state values are small, which demonstrates that the end-effector can perform soft capture if the manipulator is under the compliance control mode.

The calibration testing shows that the capture misalignment envelope of the end-effector meets the requirements. With the compliance of the robot arm, the end-effector can perform soft capture.

https://doi.org/10.1017/S0263574715000302 Published online by Cambridge University Press

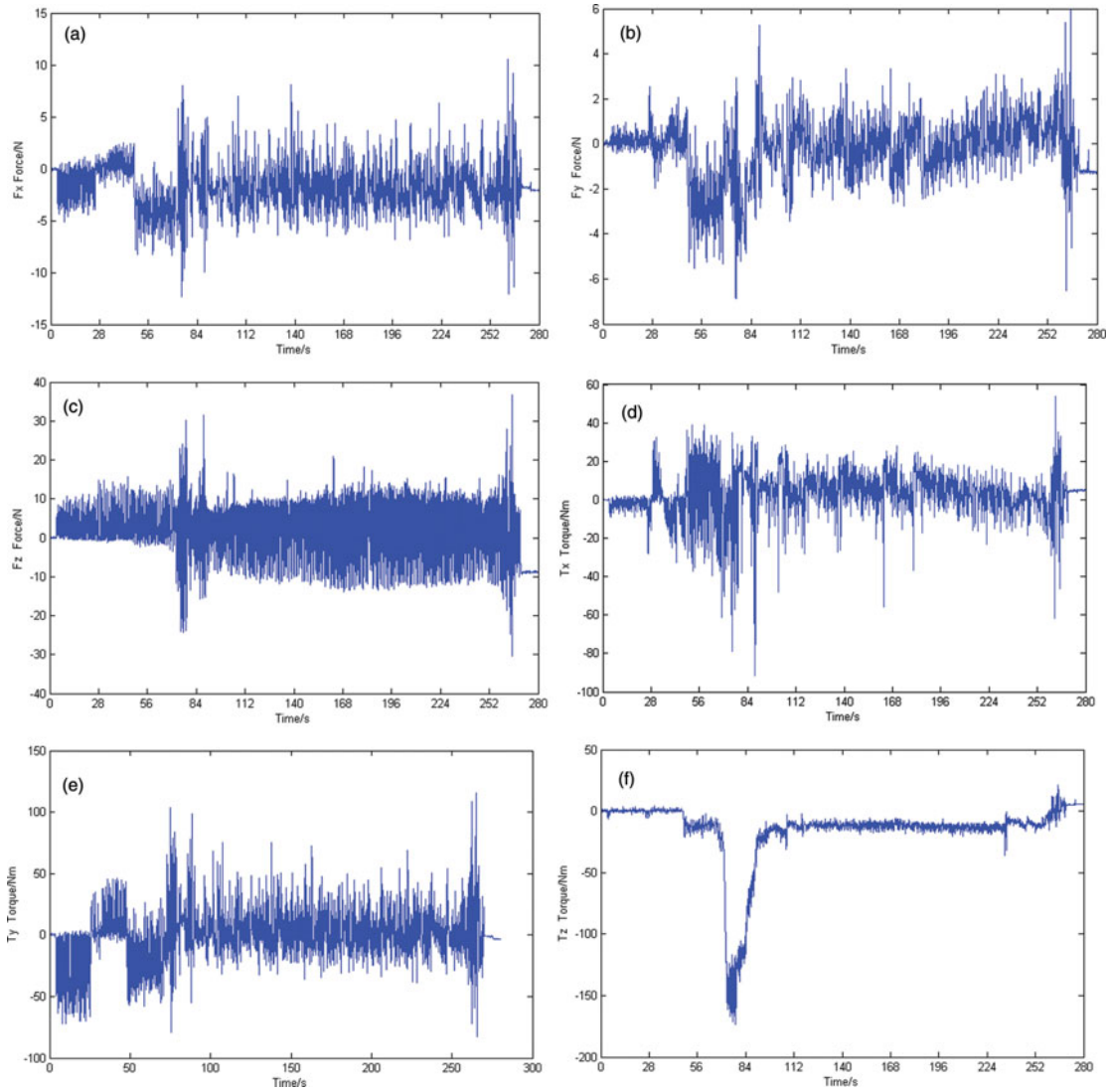

Fig. 24. Force and torque during capture operation.

5.2. *Self-relocation capture and payload handling*

The experiment is aimed at examining the end-effector's capability to support the self-relocation and payload handling of the manipulator in a simulated space environment. As shown in Fig. 25, the testing was performed on an air-bearing testbed. The platform can only simulate planar motion. In the plane, the motion is linear. In general, the operation of the manipulator has six DOFs and is nonlinear. With a "section" method, the six DOF motion can be resolved into many planar motions. The testing on the table simulates a serial of planar motions and their composition is the on-orbit operation of the manipulator.

As shown in Fig. 25, the end-effector is attached to each end of the symmetrical manipulator which is supported by three air-bearing brackets. One end-effector is attached to one of the grapple fixtures mounted on the truss base, which acts as the shoulder base of the manipulator for operation support. The end-effector of the wrist unit is used for capture. A payload is supported by an air-bearing bracket, its grapple fixture acts as a capture-point or basepoint. After the payload is located at a given position, it is static and maintains the state. The manipulator positions the end-effector by the lead of its hand-eye camera. As the grapple fixture is within the capture capability of the end-effector, the manipulator stops and switches to the compliance control mode. The control system sends a capture command and the end-effector starts and is driven by PWM. The capture fingers perform the whole capture operation. In a capture and release loop, the position tracking results of the nut are shown in

https://doi.org/10.1017/S0263574715000302 Published online by Cambridge University Press

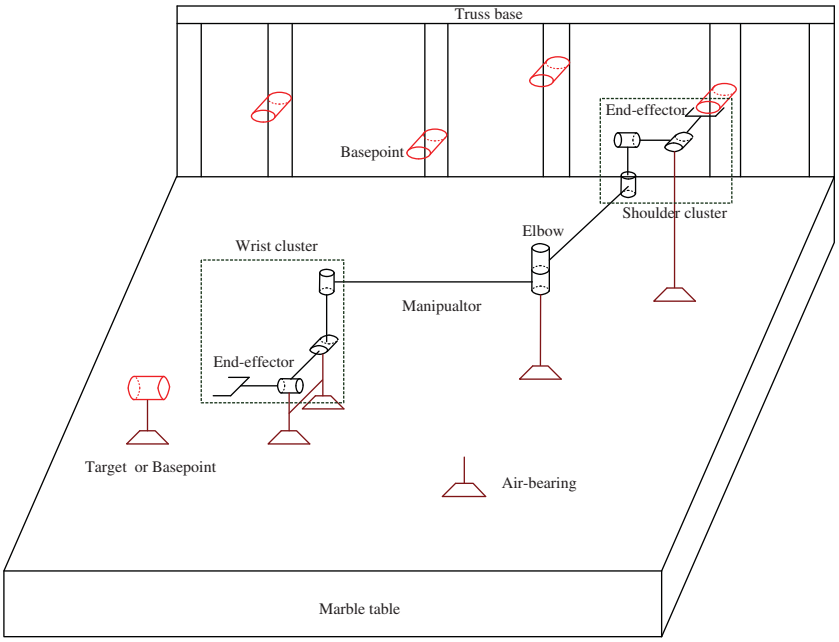

Fig. 25. Air bearing capture testing system.

Fig. 26. Its real trajectory corresponds to line 6 in Fig. 19. The tracking trajectory is subdivided into six segments and analyzed as follows.

(1) Capture operation
At the beginning, the expected position of the nut and its real position are coincidental. Once receiving a capture command, the nut starts at the maximum position of 165.374 mm. During the capture operation, the real position tracks the expected position. The tracking error changes from 0 to −2 mm. The PWM is −600. At the end of the capture operation, the real position stops at the position of 18.31 mm. It shows that the latching has been performed.

(2) Secure latching
With the mechanism constraint, the real position stops. But the expected position continues to change and the program commands the real position to continually track. The purpose is to secure the latching and eliminate the mechanical interference in the mechanism. The tracking error changes from −2 mm to −3 mm accordingly. At the outset of the change, the error curve has a spike, which shows that the position of the nut rebounds a little and then is caused to continually track the expected position. The PWM is −600.

(3) Power-off
The end-effector is powered off and the latching state is maintained. The real position still stops at 18.31 mm and the expected position stops at 15.198 mm. The tracking error retains −3 mm. The PWM is 0.

(4) Power-on
The end-effector is powered on, and the real position decreases a little and stops at 17.652 mm. In the control, the real position is the expected position. It has a light oscillation and is soon steady. The tracking error changes from −3 mm to 0 mm and stays at 0 mm. The PWM is 0.

(5) Position servo control
The end-effector is under the position servo control. The expected position stops at 17.601 mm. The real position oscillates slightly because of the sensor noise. The corresponding tracking error also oscillates and is still 0 mm. The PWM is 0.

(6) Release operation
As the release starts, the expected position and the real position change simultaneously from 17.601 mm. The expected position is ahead of the real position. The tracking error changes from

https://doi.org/10.1017/S0263574715000302 Published online by Cambridge University Press

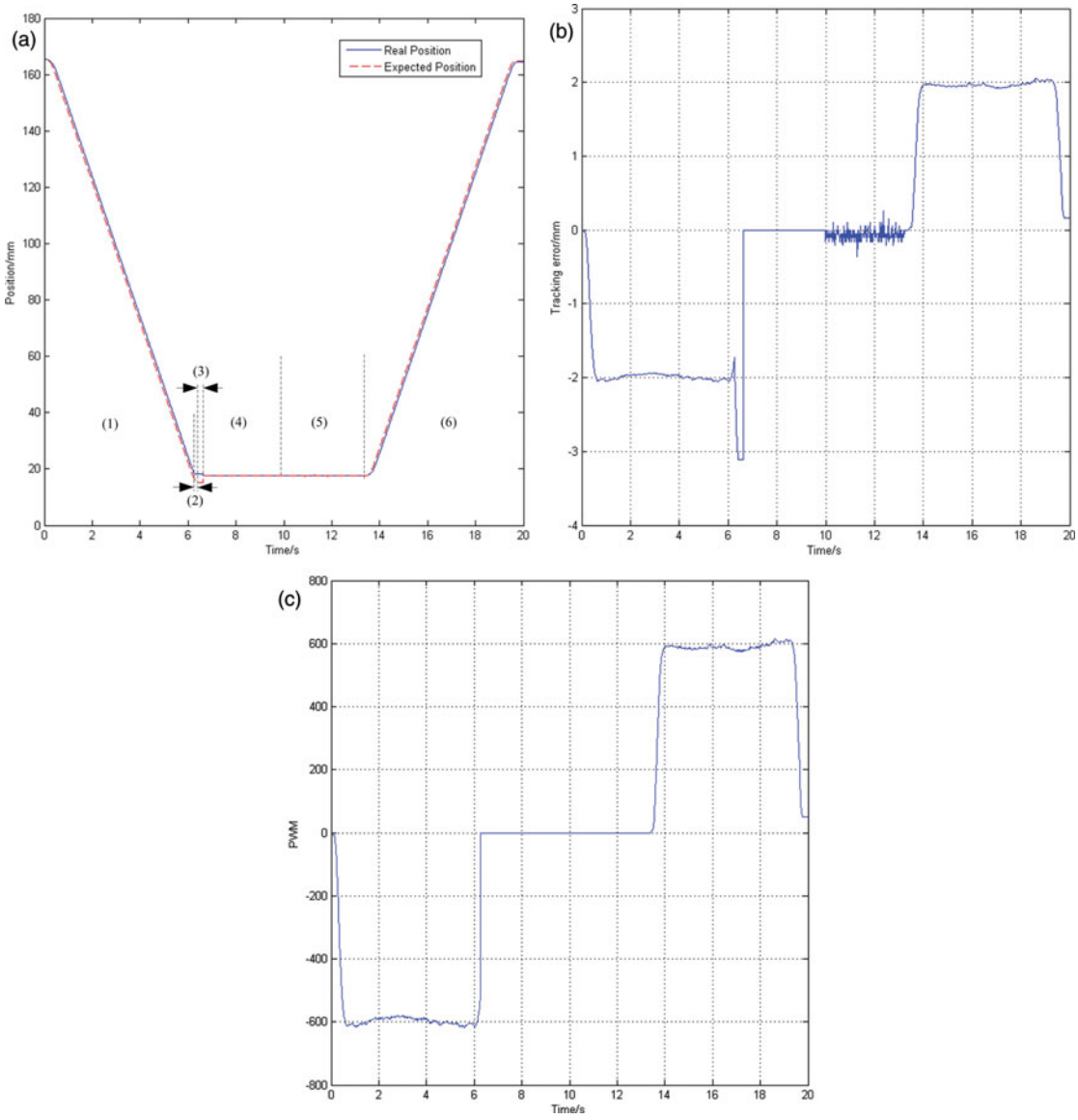

Fig. 26. Nut position tracking result and PWM. (a) Tacking trace. (b) Tracking error. (c) PWM.

0 to 2 mm. The PWM is 600. At the end of the release, the expected position stops at 165.371 mm, and the real position stops at 165.204 mm. The purpose is to make the nut reach the final position. The tracking error changes from 2 mm to 0.167 mm. The PWM is 0.

The results demonstrate that the position servo control for the end-effector can secure the capture, dragging, latching and release. The testing also demonstrates that the end-effector of the manipulator under the zero force control mode can softly capture the grapple fixture which is attached to the payload or as a basepoint.

6. Conclusions

An end-effector was developed. Its characteristics and suitability were analyzed and validated by a series of simulations and experiments. The simulation results show that the misalignment envelope of the end-effector meets the requirements of the free floating target capture. The comparisons between the simulation and testing demonstrate that it enlarges greatly when the grapple fixture (target) is constrained or fixed. The simulation and the testing illustrate the capture failure from two points of view. They also demonstrate that the analytic criterions and methods are very effective for the

https://doi.org/10.1017/S0263574715000302 Published online by Cambridge University Press

end-effector, and the capture operation must perform in the safe capture space. For OOS, the soft docking and soft capture are of vital importance. They are realized by the spring-damper systems built into the end-effector and by the compliance motion of the manipulator, respectively. Being attached to two ends, the end-effector can support the self-relocation and payload handling of the manipulator. During the self-relocation capture and payload capture, the manipulator is in the close link state so that the capture operation velocity should be slow. An axial separate velocity between the end-effector and grapple fixture is required and comes with the release velocity of the capture fingers. The testing shows that the end-effector satisfies the requirements and it can work well in a simulated space environment.

Further work focuses on the refined testing, contact dynamics modeling and managing.

Acknowledgements

This project is supported by National Key Basic Research Program of China (973 Program, Grant No. 2013CB733103).

References

1. D. King, "Space Servicing: Past, Present and Future[C]," *Proceeding of the 6th International Symposium on Artificial Intelligence and Robotics & Automation in Space*, St–Hubert, Quebec, Canada, (Jun. 18–22, 2001) pp. 1–8.
2. G. Hirzinger, B. Brunner and R. Lampariello et al., "Advances in Orbital Robotics[C]," *Proceedings of the IEEE Conference on Robotics & Automation*, San Francisco, CA, (Apr. 2000), vol. 1, pp. 898–907.
3. E. Stoll, J. Letschnik and U. Walter et al., "On-orbit servicing[J]," *IEEE Robot. Autom. Mag.* **16**(4), 29–33 (2009).
4. D. Finkleman and D. Oltrogge, "Twenty-five Years, More or Less?[C]," *Proceedings of the AIAA/AAS Astrodynamics Specialist Conference*, Toronto, Ontario Canada, (Aug. 2–5, 2010) pp. 1–14.
5. G. Hirzinger, K. Landzettel, B. Brunner et al., "DLR's robotics technologies for on-orbit servicing[J]," *Adv. Robot.* **18**(2), 139–174 (2004).
6. R. Rembala and C. Ower, "Robotic assembly and maintenance of future space stations based on the ISS mission operations experience[J]," *Acta Astronaut.* **65**(7), 912–920 (2009).
7. H. A. Thronson, D. Akin and J. Grunsfeld et al., "The Evolution and Promise of Robotic in-space Servicing[C]," *Proceedings of the AIAA SPACE 2009 Conference & Exposition*, Pasadena, California, (Sept. 14–17, 2009) pp. 1–6.
8. B. J. Roberts, "Using the International Space Station as a Precursor to In–Orbit Robotic Servicing[C]," *Proceedings of the AIAA SPACE 2010 Conference & Exposition*, Anaheim, California, (Aug. 30–Sept. 2, 2010) pp. 1–8.
9. D. M. Gossain and S. S. Sachdev, Self-relocating manipulator, US Patent 4,585,388[P]. 1986-4-29.
10. L. R. Purves, Robot serviced space facility, US Patent 5,145,130[P]. 1992-9-8.
11. T. Haidegger, "Advanced Robotic Arms in Space[C]," *Proceedings of the 55th International Astronautical Congress Vancouver*, Canada, (2004) pp. 1–10.
12. P. Laryssa, E. Lindsay and O. Layi et al., "International Space Station Robotics: A Comparative Study of ERA, JEMRMS and MSS[C]," *Proceedings of the 7th ESA Workshop on Advanced Space Technologies for Robotics and Automation, Noordwijk*, Netherlands, (Nov. 19–21, 2002) pp. 1–8.
13. C. Sallaberger, "Force S P T. Canadian space robotic activities[J]," *Acta Astronaut.* **41**(4), 239–246 (1997).
14. P. J. Lambooy, W. M. Mandersloot and R. H. Bentall, "Some Mechanical Design Aspects of the European Robotic Arm[C]," *Proceedings of the 29th Aerospace Mechanisms Symposium. Johnson Space Center*, Houston, Texas, (1995), vol. 1, pp. 17–29.
15. S. Nishida and T. Yoshikawa, "A New End-effector for On-orbit Assembly of a Large Reflector[C]," *Proceedings of the IEEE Conference on Control, Automation, Robotics and Vision*, Singapore, (Dec. 5–8, 2006) pp. 1–6.
16. R. Kumar and R. Hayes, "System Requirements and Design Features of Space Station Remote Manipulator System mechanisms[C]," *Proceedings of the 25th Aerospace Mechanisms Symposium*, Washington, DC, (May, 1991) pp. 15–30.
17. E. Quittner, R. Vandersluis and J. Rakhsha et al., "System and Concept Design of the SSRMS Latching End-effector[C]," *Proceedings of the 3rd European Space Mechanism & Tripology Symposium*, Madrid, Spain, (Sept. 30–Oct. 2, 1987) pp. 93–103.
18. B. Walker and R. Vandersluis, "Design, Testing and Evaluation of Latching End-effector[C]," *Proceedings of the 29th Aerospace Mechanisms Symposium, Johnson Space Center*, Houston, Texas, (1995) pp. 1–16.
19. D. G. Hunter, "The Space Station Freedom special Purpose Dexterous Manipulator (SPDM)[C]," *Proceedings of the IEEE National Telesystems Conference*, NTC'91, Atlanta, GA, (Mar. 26–27, 1991), vol. 1, pp. 371–376.
20. C. J. Hwang, Design of a robotic end-effector to emulate the orbit replaceable unit/tool change-out mechanism (OTCM) for space station robotic system[J]. (1996), pp. 1–8. http://www.tern.com/portal/library/nasa_mc.pdf

21. R. Boumans and C. Heemskerk, "The European robotic arm for the international space station[J]," *Robot. Auton. Syst.* **23**(1), 17–27 (1998).
22. F. Doctor, A. Glas and Z. Pronk, "Mission Preparation Support of the European Robotic Arm (ERA)[C]," *Proceedings of the 7th ESA Workshop on Advanced Space Technologies for Robotics and Automation*, Noordwijk, Netherlands, (Nov. 19–21, 2002) pp. 1–8.
23. C. J. M. Heemskerk, M. Visser and D. Vrancken, "Extending ERA's Capabilities to Capture and Transport Large Payloads[C]," *Proceedings of the 9th ESA Workshop on Advanced Space Technologies for Robotics and Automation*. Noordwijk, Netherlands, (Nov. 28–30, 2006) pp. 1–8.
24. S. Michaud, M. Dominguez, U. Nguyen, L. Zago and S. Droz, "Eurobot End-effectors[C]," *Proceedings of the 8th ESA Workshop on Advanced Space Technologies for Robotics and Automation, 'ASTRA 2004' ESTEC*, Noordwijk, The Netherlands, (Nov. 2–4, 2004) pp. 1–8.
25. R. Gelmi, A. Rusconi and J. F. G. Lodoso et al., "Design of a Compact Tool Exchange Device for Space Robotics Applications[C]," *Proceedings of the 9th ESA Workshop on Advanced Space Technologies for Robotics and Automation, 'ASTRA 2006' ESTEC*, Noordwijk, The Netherlands, (Nov. 28–30, 2006) pp. 1–7.
26. J. F. Andary and P. D. Spidaliere, "The development test flight of the flight telerobotic servicer: Design description and lessons learned[J]," *IEEE Trans. Robot. Autom.* **9**(5), 664–674 (1993).
27. G. Hirzinger, B. Brunner and J. Dietrich et al., "Sensor-based space robotics-ROTEX and its telerobotic features[J]," *IEEE Trans. Robot. Autom.* **9**(5), 649–663 (1993).
28. S. Kimura, T. Okyuama and N. Yoshioka et al., "Robot-aided remote inspection experiment on STS-85[J]," *IEEE Trans. Aerosp. Electron. Syst.* **36**(4), 1290–1297 (2000).
29. M. Oda, "Experiences and Lessons Learned from the ETS-VII Robot Satellite[C]," *Proceedings of IEEE International Conference on Robotics and Automation, ICRA'00.* San Francisco, CA, (Apr. 24–28, 2000), vol.1, pp. 914–919.
30. T. Matsueda, K. Kuraoka and K. Goma et al., "JEMRMS System Design and Development Status[C]," *Proceedings of the IEEE National Telesystems Conference(NTC'91),* Atlanta, GA, (Mar. 26–27, 1991), vol. 1, pp. 391–395.
31. H. Akatsuka, H. Ogasawara and H. Endoh et al., "Development of End-effector and Grapple Fixture for the Small Fine Arm of 'Kibo'[C]," *Proceedings of the twenty-third international symposium on space technology and science(Selected papers)*, Matsue, Shimane, Japan, (May 26–Jun 31, 2002), vol 2, pp. 1503–1508.
32. A. Tsuchihashi, N. Noguchi, K. Kuraoka. End-effector: US Patent 4,955, 654[P]. 1990-9-11.
33. M. Oda, M. Nishida and S. Nishida, "Development of an EVA End-effector, Grapple Fixtures and Tools for the Satellite Mounted Robot System[C]," *Proceedings of the IEEE/RSJ International Conference on Intelligent Robots and Systems*, Osaka, Japan, (Nov. 4–8, 1996), vol. 3, pp. 1536–1543.
34. G. Hirzinger, B. Brunner and K. Landzettel et al., "Preparing a New Generation of Space Robots-a Survey of Research at DLR[J]," *Robot. Auton. Syst.* **23**, 99–106 (1998).
35. A. Rusconi, R. Finotello, G. Borghi, R. Mugnuolo, A. Olivieri and F. Pasquali, "EUROPA (External use of Robotics for Payloads Automation)[C]," *Proceedings of the AIAA SPACE 2001 Conference and Exhibit on International Space Station Utilization*, Cape Canaveral, FL, (Oct. 15–18, 2001) pp. 1–10.
36. R. Mugnuolo, S. Di Pippo and P. G. Magnani et al., "The SPIDER manipulation system (SMS) The Italian approach to space automation[J]," *Robot. Auton. Syst.* **23**(1), 79–88 (1998).
37. B. Rubinger et al., "A Novel Robotic Hand-SARAH For Operations on the International Space Station[C]," *Proceedings of the 7th ESA Workshop on Advanced Space Technologies for Robotics and Automation 'ASTRA 2002*', ESTEC, Noordwijk, The Netherlands, (Nov. 19–21, 2002) pp. 1–8.
38. J. C. Parrish, B. R. Sullivany and B. J. Robertsz, "Planning for the Ranger Telerobotic Shuttle Experiment on-orbit Operations," *AIAA Space 2000, AIAA 2000–5291*, Long Beach, (Sept. 2000) pp. 1–9.
39. Q.. Liu, *Research on End-Tools Exchange Device of Space Robot[D]*, (Harbin Institute of Technology, Harbin, 2011). (in Chinese)
40. L. Ren, *Design of a New Exchange Device and Research on its Manipulating Strategy[D]*, (Harbin Institute of Technology, Harbin, 2012). (in Chinese).
41. H. Liu, Y. Tan, and Yi-wei Liu et al., "Development of chinese large-scale space end-effector[J]," *J. Cent. South Univ. Technol.***18**, 600−609 (2011).
42. F. Feng, Y. Liu, H. Liu and H. Cai, "Design schemes and comparison research of the end-effector of large space manipulator[J]," *CJME* **25**(4), 674–687 (2012).
43. Q. Zhang, F. L. Ni, and Y. Zhu et al., "Compliant grasp strategy for three-fingered space robot end-effector[J]," *Robot* **33**(4), 427–433 (2011). (in Chinese).
44. F. Feng, Y. Liu and H. Liu et al., "Design and simulation analysis of a space end-effector with large misalignment tolerance [J]," *Robot* **33**(6), 691–699 (2011), (in Chinese).
45. S. Christiansen and T. Nilson, "Docking System for Autonomous, Un-manned Docking Operations[C]," *Proceedings of the IEEE Conference on Aerospace*, Big Sky, MT, (Mar. 1–8, 2008) pp. 1–14.
46. P. Motaghedi and S. Stamm, "6 DOF Testing of the Orbital Express Capture System[C]," *Defense and Security. International Society for Optics and Photonics*, Bellingham, WA, (2005), vol. 5799, pp. 66–81.
47. P. Motaghedi, "On-Orbit Performance of the Orbital Express Capture System[C]," *SPIE Defense and Security Symposium. International Society for Optics and Photonics*, Orlando, FL, (Mar. 16, 2008) vol. 6958, pp. 1–12.

48. S. Stamm and P. Motaghedi, "Orbital Express Capture System: Concept to Reality[C]," *Defense and Security. International Society for Optics and Photonics*, Bellingham, WA, (Aug. 2004) pp. 78–91.
49. G. Gottselig, "Orbital Express Advanced Technology Demonstration[C]," *Presentation to 2002 Core Technologies for Space Systems Conference*, (2002) pp. 19–21.
50. H. Ueno, Y. Wakabayashi and H. Morimoto et al., "Berthing Load Analysis between Space Manipulator and Berthing Mechanism during On-orbit Assembly Operation[C]," *Proceedings of the 9th International Symposium on Artificial Intelligence and Robotics & Automation in Space*, Hollywood, USA, (Feb. 26–29, 2008) pp. 1–6.
51. J. S. Dai, D. L. Wang and L. Cui, "Orientation and workspace analysis of the multifingered metamorphic hand—Metahand," *IEEE Trans. Robot.* **25**(4), 942–947 (2009).
52. G. Wei, J. S. Dai, S. Wang and H. Luo, "Kinematic analysis and prototype of a metamorphic anthropomorphic hand with a reconfigurable palm," *Int. J. Humanoid Robot.* **8**(3), 459–479 (2011).

Appendix: definitions of the parameters

a, b, c, d, e—Lengths of the line segments FI, IQ, QN, AW and IW, respectively

d_1—Distance between the w-axis and the hemline of the interface plate

d_2—Distance between the z-axis and the limiting position of the point B

d_{GE}—Distance between the grapple fixture and the end-effector

d_{FG}—Distance between the capture fingers the grapple fixture

d_{GL}—Distance between the linking hooks the grapple fixture

h_{S}—Height of the capture feature space

h_{T}—Thickness of the interface plate

L_{MB}, L_{DE}, L_{BE}, L_{DJ}—Lengths of the line segments MB, DE, BE and DJ, respectively

L_{JB}, r, r_C, $r_F(=x_F)$—Radiuses of the point B, the latching roller, the semi-circle trough of the linking hook and the capture finger tip point F, respectively

L, l—Lengths of the wedge surface and the hemline of the interface plate

n—Distance between the point N and the z-axis

R_1, R_2—Internal and external radius of the capture feature space, respectively

R_{E}—Radius of the end-effector

S_N—Displacement of the point N

S_{Fs}, Θ—Sliding displacement and angular displacement of the capture finger during capture phase

$S(\gamma)$, $S^{-1}(s)$—Transfer function and its inverse function of the mechanism

δ—Angle of the interface plate slop

α—Angle between the lines MB and BE, α_0 is the initial value

α_{P}—Pressure angle of the linkage mechanism

β_0—Angle between the lines BE and JB, β_0 is a constant

γ—Angle between the line BE and the x-axis, γ_0 is the initial value

Φ—Angle between the line NH and the z-axis

χ—Angle between the line NJ and the z-axis

θ_L—Angle between the lines DJ and BE

θ_T—Angle between the lines JT and JK

β—Angle between the radius $O_{\mathrm{G}}A_1$ and the plane $O_{\mathrm{G}}F_1I_1$

ε—Angle between the radius $O_{\mathrm{G}}A_1$ and the radius $O_{\mathrm{G}}D_1$

$\gamma_{\min}$—Minimum driving angle of the linkage mechanism

https://doi.org/10.1017/S0263574715000302 Published online by Cambridge University Press

$\Delta\gamma$—Angular displacement of the latching finger

m_{C}—Mass of the capture finger

μ_1, μ_2—Friction coefficient between the capture finger and the guide pin, the latching roller and the grapple fixture, respectively

J_{LJ}—Moment of inertia of the latching mechanism about the axis of the guide pin

F_N, F_G, N_J, f_J, N_s, f_s, N_L—Forces acting on the capture finger

N'_L, F_{LR}, N_{JL}, f_{JL}—Forces acting on the latching mechanism

v_{CF}, v_{GF}, v_{EE}—Velocity of the capture finger, the grapple fixture and the end-effector, respectively

v_{Tz}—Projection of the velocity of the point T of tangency on the y-axis

https://doi.org/10.1017/S0263574715000302 Published online by Cambridge University Press